Neuron
Article

# Suppression of Neurodegeneration and Increased Neurotransmission Caused by Expanded Full-Length Huntingtin Accumulating in the Cytoplasm

Eliana Romero,[1,7] Guang-Ho Cha,[1,7] Patrik Verstreken,[1,2,4,7,8] Cindy V. Ly,[3] Robert E. Hughes,[6] Hugo J. Bellen,[1,2,3,4] and Juan Botas[1,5,*]
[1]Department of Molecular and Human Genetics
[2]Howard Hughes Medical Institute
[3]Department of Neuroscience
[4]Program in Developmental Biology
[5]Department of Molecular and Cellular Biology
Baylor College of Medicine, Houston, TX 77030, USA
[6]Buck Institute, 8001 Redwood Boulevard, Novato, CA 94945, USA
[7]These authors contributed equally to this work.
[8]Present address: VIB Department of Molecular and Developmental Genetics, Katholieke Universiteit Leuven Department of Human Genetics, Herestraat 49, bus 602, B3000 Leuven, Belgium.
*Correspondence: jbotas@bcm.tmc.edu
DOI 10.1016/j.neuron.2007.11.025

## SUMMARY

**Huntington's disease (HD) is a dominantly inherited neurodegenerative disorder caused by expansion of a translated CAG repeat in the N terminus of the huntingtin (htt) protein. Here we describe the generation and characterization of a full-length HD *Drosophila* model to reveal a previously unknown disease mechanism that occurs early in the course of pathogenesis, before expanded htt is imported into the nucleus in detectable amounts. We find that expanded full-length htt (128Qhtt$^{FL}$) leads to behavioral, neurodegenerative, and electrophysiological phenotypes. These phenotypes are caused by a $Ca^{2+}$-dependent increase in neurotransmitter release efficiency in 128Qhtt$^{FL}$ animals. Partial loss of function in synaptic transmission (syntaxin, Snap, Rop) and voltage-gated $Ca^{2+}$ channel genes suppresses both the electrophysiological and the neurodegenerative phenotypes. Thus, our data indicate that increased neurotransmission is at the root of neuronal degeneration caused by expanded full-length htt during early stages of pathogenesis.**

## INTRODUCTION

Expansion of the glutamine tract of huntingtin (htt) invariably leads to psychiatric, motor, and cognitive disturbances. Most Huntington's disease (HD) patients become symptomatic late in life, but large expansions of the glutamine tract (>70 repeats) lead to juvenile forms of the disease, which demonstrates an inverse relationship between repeat size and disease onset (The Huntington's Disease Collaborative Research Group, 1993). Glutamine-expanded htt forms ubiquitin-positive aggregates in the nuclei and neurites of brain neurons (DiFiglia et al., 1997; Rubinsztein, 2002). Wild-type htt is a large (350 kDa) soluble protein that is conserved between *Drosophila* and mammals and is detected in neurons and other cell types. Htt is most abundant in the cytoplasm, where it associates with the Golgi complex, endoplasmic reticulum, and synaptic vesicles (Cattaneo et al., 2005). Although essential for murine embryogenesis (Nasir et al., 1995), its normal functions are still poorly understood. Protein interaction analyses implicate htt in diverse processes, including intracellular trafficking, axonal transport, transcriptional regulation, cytoskeletal organization, and prevention of apoptosis (Goehler et al., 2004; Harjes and Wanker, 2003; Kaltenbach et al., 2007; Li and Li, 2004b). Htt has also been linked to neurotransmission (reviewed in Harjes and Wanker, 2003; Li et al., 2003; Smith et al., 2005). For example, htt associates with clathrin-coated pits and vesicles at synaptic terminals (DiFiglia et al., 1995; Velier et al., 1998). Increased neuronal input resistance, lower stimulus intensity to evoke action potentials (Klapstein et al., 2001), impaired long-term potentiation (Hodgson et al., 1999; Klapstein et al., 2001; Murphy et al., 2000; Usdin et al., 1999), and abnormal responses to NMDA stimulation (Cepeda et al., 2001; Laforet et al., 2001) in HD neurons suggest that synaptic dysfunction may contribute to pathogenesis. Studies in the R6/2 N-terminal mouse model have shown alterations in the corticostriatal pathway and altered levels of postsynaptic markers (Cepeda et al., 2003). However, it is unclear whether alterations in synaptic function are early events or secondary to neuronal dysfunction during pathogenesis.

Mouse models for HD include transgenic animals expressing either truncations of htt or the entire protein, and "knockins" expressing the endogenous murine protein with an expanded polyglutamine tract (reviewed in Menalled, 2005; Menalled and Chesselet, 2002; Rubinsztein, 2002). Most studies have been conducted using the first generated models that only express a small N-terminal portion of the protein (exon 1) containing the polyglutamine expansion. Mice expressing short truncations of

the expanded protein typically have earlier and more severe phenotypes than mice expressing the entire protein. They also show formation of nuclear aggregates early in life. Full-length or longer N-terminal models exhibit cytoplasmic accumulation of htt, and the nuclear localization or aggregation occurs only later in life (Hickey and Chesselet, 2003; Menalled, 2005; Menalled et al., 2002; Rubinsztein, 2002; Van Raamsdonk et al., 2005). Moreover, N-terminal mouse models fail to reproduce the specificity of neuronal degeneration observed in HD patients, where neuronal loss occurs mainly in the striatum and cortex (Li and Li, 2004a). This selective neurodegeneration is best reproduced in models that express the full-length protein (Van Raamsdonk et al., 2005).

*Drosophila* HD models have been used to demonstrate that nuclear (i.e., transcriptional dysregulation [Steffan et al., 2001]), and nonnuclear (i.e., fast axonal transport [Lee et al., 2004]) mechanisms of pathogenesis, as well as posttranslational modifications of htt, are important for pathogenesis (Steffan et al., 2004). They have also been used to identify chemical compounds that may ameliorate htt-induced toxicity (Bilen and Bonini, 2005; Marsh and Thompson, 2004; Sang and Jackson, 2005). However, no full-length model of HD has been reported in *Drosophila*.

Studies using N-terminal models have provided many important insights into HD; however, it is clear that protein context is important for pathogenesis (Yu et al., 2003). This is best illustrated by a transgenic mouse expressing 120 CAG repeats in the context of exons 1 and 2 of the htt protein, which shows no neuronal dysfunction or degeneration despite abundant neuronal inclusions (Slow et al., 2005). The importance of appropriate protein context has also been documented in the case of other polyglutamine diseases (Gatchel and Zoghbi, 2005).

Here we report the development of a full-length *Drosophila* HD model to investigate the mechanisms by which expanded full-length htt impairs synaptic transmission. We show that expression of expanded full-length htt leads to an increased neurotransmitter release efficiency. This phenotype can be suppressed genetically by removing a single copy of the genes encoding the proteins that are required for proper neurotransmitter release. We find that resting intracellular $Ca^{2+}$ levels are increased in these flies when compared to controls. This suggests a defect in $Ca^{2+}$ homeostasis, which is in agreement with observations in mammalian systems (Bezprozvanny and Hayden, 2004; Cepeda et al., 2001; Hodgson et al., 1999; Tang et al., 2005). Importantly, these abnormalities occur before we can detect the cleavage and nuclear translocation of the htt protein. We also show that mutations in certain voltage-gated $Ca^{2+}$ channels restore the elevated $Ca^{2+}$ levels and improve neurotransmitter release efficiency and neurodegenerative phenotypes.

## RESULTS

### Full-Length Human htt Accumulates in the Cytoplasm of *Drosophila* Neurons and Does Not Form Visible Aggregates

We generated transgenes to express the entire 3144 aa human protein with either 16 (16Qhtt$^{FL}$, wild-type) or 128 (128Qhtt$^{FL}$, pathogenic) glutamines under the control of the UAS-GAL4 system (Brand and Perrimon, 1993). Western analyses revealed a band corresponding to the ~350 kDa full-length protein in *Drosophila* expressing either the 16Qhtt$^{FL}$ or the 128Qhtt$^{FL}$ transgenes with the GMR-GAL4 eye driver. In contrast, no such protein was detected in GMR-GAL4 controls. The 16Qhtt$^{FL}$ protein runs slightly faster than the 128Qhtt$^{FL}$ protein, as may be expected from the different number of glutamine repeats (Figure 1A).

To determine the intracellular localization of full-length htt in *Drosophila,* we used a GAL4 driver directing expression to a specific subset of large central nervous system (CNS) neurons, the ap$^{VNC}$ interneurons (Fernandez-Funez et al., 2000). Labeling using MAB5374 shows cytoplasmic accumulation of both 16Qhtt$^{FL}$ and 128Qhtt$^{FL}$ in ap$^{VNC}$ interneurons of 20-day-old flies (Figure 1B, left and central panels). Similar results were observed in 10-day-old and 30-day-old flies (data not shown). The absence of detectable nuclear htt staining is not a consequence of this antibody's inability to detect htt in the nucleus because flies expressing an N-terminal truncated form of the protein (amino acids 1–208) with the same glutamine expansion show robust nuclear staining using the same antibody concentration and experimental conditions (Figure 1B, right panels; see also Jackson et al. [1998] and Steffan et al. [2001] for nuclear staining of similarly sized htt fragments in *Drosophila*). Thus, the cytoplasmic accumulation of 128Qhtt$^{FL}$ is reminiscent of data from HD murine models wherein full-length htt localizes to the cytoplasm first, and nuclear staining is only evident months after birth (Menalled, 2005; Rubinsztein, 2002; Slow et al., 2003), a time well beyond the lifespan of flies.

We subsequently investigated whether full-length htt forms aggregates in *Drosophila* neurons. Large axonal aggregates blocking axonal transport have been reported in flies expressing an expanded N-terminal htt fragment of 548 amino acids (Lee et al., 2004). In contrast to 128Qhtt$^{1-548}$ (Figure 1C, lower right panel), 128Qhtt$^{FL}$ does not form obvious axonal aggregates (Figure 1C, lower left panel). To investigate whether axonal transport is impaired in 128Qhtt$^{FL}$ flies, we monitored the localization of synaptotagmin I, a synaptic vesicle-associated protein that is transported along axons (Lee et al., 2004). We found that in animals expressing 128Qhtt$^{1-548}$, synaptotagmin I, like htt, accumulates in the axons (Figure 1D, lower right panel). In contrast, larvae expressing the control protein GFP (Figure 1D, upper left panel) or the full-length htt protein (expanded or unexpanded) (Figure 1D, lower left and upper right panels, respectively) do not show accumulation of synaptotagmin I in axons. Thus, although it is difficult to exclude the possibility of decreased axonal transport, we found no evidence of axonal blockages disrupting transport in 128Qhtt$^{FL}$-expressing animals.

### Expression of 128Qhtt$^{FL}$, but Not 16Qhtt$^{FL}$, in the *Drosophila* Eye and CNS Leads to Progressive Neurodegenerative Phenotypes

To examine the consequences of expressing full-length htt in the visual system, the 16Qhtt$^{FL}$ and 128Qhtt$^{FL}$ transgenes were expressed using GMR-GAL4 drivers. Examination of the external eye morphology using light microscopy and scanning electron microscopy (SEM) revealed depigmentation and disorganization of ommatidia following expression of 128Qhtt$^{FL}$(s) but not

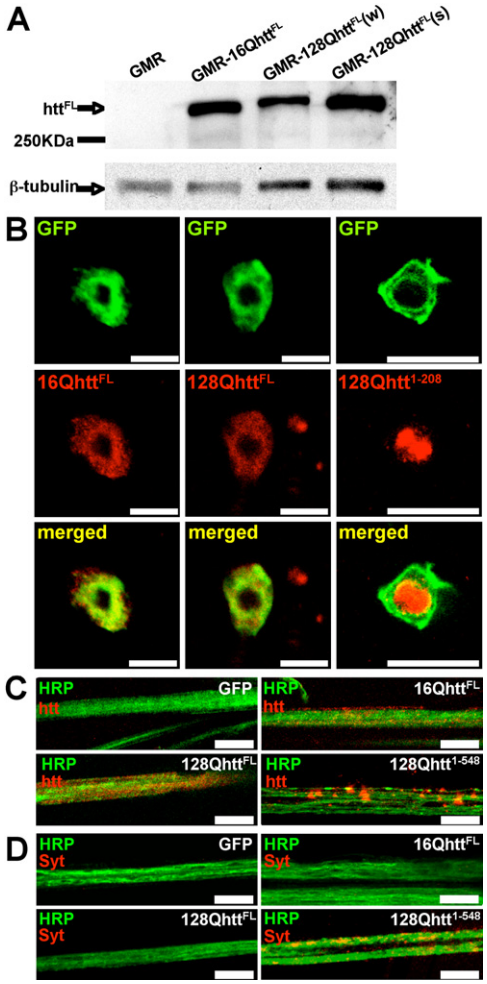


**Figure 1. Human Full-Length htt Accumulates in the Cytoplasm of *Drosophila* Neurons and Does Not Form Visible Axonal Aggregates**

(A) Western analysis of transgenic *Drosophila* heads using MAB2166 reveals a (~350 KDa) band corresponding to full-length (unexpanded and expanded) human htt. Based on densitometry analysis, the 16Q line expresses higher/similar protein levels than the 128Q(w) and 128Q(s) lines (~2-fold and ~1-fold, respectively). Genotypes: GMR (*GMR-GAL4/UAS-GFP*), GMR-16Qhtt$^{FL}$ (*GMR-GAL4/UAS-16Qhtt$^{FL}$[M28]*), GMR-128Qhtt$^{FL}$(w) (*GMR-GAL4/+; UAS-128Qhtt(w)[F7]/+*), GMR-128Qhtt$^{FL}$(s) (*GMR-GAL4/UAS-128Qhtt(s)[M36E2]*).

(B) Immunofluorescence confocal images of *Drosophila apterous* ventral nerve cord interneurons from 20-day-old flies expressing wild-type (left, 16Qhtt$^{FL}$) or expanded (middle, 128Qhtt$^{FL}$) full-length htt. Right panels show similar images from animals expressing an expanded N-terminal htt truncation (amino acids 1–208 excluding the polyglutamine tract, 128Qhtt$^{1-208}$). Note colocalization of full-length htt with the CD8-GFP cytoplasmic marker. The same results were obtained with 10-day-old and 30-day-old flies (data not shown). In contrast, 128Qhtt$^{1-208}$ accumulates in the nucleus as early as the third-instar larval stage. MAB5374 was used at 1:100 for all stainings, which were done simultaneously. Flies raised at 27°C. Scale bar, 5 μm. Genotypes: 16Qhtt$^{FL}$ (*UAS-16Qhtt$^{FL}$[M28]/UAS-CD8-GFP; apVNC-GAL4/+*), 128Qhtt$^{FL}$ (*UAS-128Qhtt$^{FL}$(s)[M36E2]/UAS-CD8-GFP; apVNC-GAL4/+*), 128Qhtt$^{1-208}$ (*UAS-CD8-GFP/+; UAS-128Qhtt$^{1-208}$[M64]/apVNC-GAL4*).

(C and D) Immunolabeling of htt (C) or endogenous synaptotagmin I (Syt) (D) proteins in motor neuron axon bundles from third-instar larvae of the genotype indicated in each panel. Note diffuse pattern and absence of aggregates in wild-type (16Qhtt$^{FL}$) and expanded htt (128Qhtt$^{FL}$) axons. In contrast, a long N-terminal htt truncation (amino acids 1–548, 128Qhtt$^{1-548}$) causes large htt and synaptotagmin I axonal aggregates. MAB5374 1:100. Flies were at 29°C. Scale bar, 5 μm. Genotypes: GFP (*Elav-GAL4/+; UAS-GFP/+*), 16Qhtt$^{FL}$ (*Elav-GAL4/+; UAS-16Qhtt$^{FL}$[M28]/+*), 128Qhtt$^{FL}$ (*Elav-GAL4/+; UAS-128Qhtt$^{FL}$(s)[M36E2]/+*), 128Qhtt$^{1-548}$ (*Elav-GAL4/+; UAS-128QHtt$^{1-548}$/+*).

16Qhtt$^{FL}$ from GMR-GAL4(s), a relatively strong driver (Figures 2A–2D, left and center panels).

To investigate whether the eye phenotype is progressive, the same htt transgenes were expressed using a weaker GMR-GAL4 eye driver to facilitate comparison of the internal retinal structure between animals of different genotypes. Phalloidin staining of dissected wild-type eyes reveals the organization of the *Drosophila* eye in ommatidia. Each ommatidium contains eight rhabdomeres (the rod-shaped structures where the photopigment rhodopsin accumulates in photoreceptor neurons), seven of which are typically visible in a single plane (Figure 2A, right panel). Because retinal degeneration often results in fewer rhabdomeres, we compared the number of rhabdomeres per ommatidium in 1-day-old and 20-day-old animals expressing 128Qhtt$^{FL}$, 16Qhtt$^{FL}$, or a lacZ control transgene. In 1-day-old flies, we observed no differences between the distributions of rhabdomeres in these genotypes, with seven rhabdomeres visible in most ommatidia (Figure 2E). However, in flies aged for 20 days, we found significantly fewer rhabdomeres in 128Qhtt$^{FL}$ flies than in 16Qhtt$^{FL}$ and lacZ control flies (right panels of Figures 2A–2D and Figure 2F, $p < 0.0001$, Mann-Whitney test). Thus, the analyses of both external and internal eye phenotypes caused by full-length htt using two GMR-GAL4 drivers of different strengths yielded similar results. Furthermore, expression of 128Qhtt$^{FL}$ leads to progressive degeneration of photoreceptor cells.

We also investigated the consequences of expressing 128Qhtt$^{FL}$ in CNS neurons. First, we compared the survival rates of 128Qhtt$^{FL}$ and GFP control animals following transgene expression in motor neurons using the C164-GAL4 driver (Pennetta et al., 2002). As shown in Figure 3A, flies expressing 128Qhtt$^{FL}$ show reduced survival in adult life when compared with controls expressing GFP ($p < 0.05$, $p < 0.01$, and $p < 0.01$ for days 25, 30, and 35, respectively, Mann-Whitney test).

We then compared motor performance in 128Qhtt$^{FL}$ and control animals. First we measured motor performance in a climbing assay that exploits the strong negative geotaxis behavior of *Drosophila*. This assay measures the ability of flies to climb a vial wall as a function of age. As shown in Figure 3B, we found impaired motor performance in 128Qhtt$^{FL}$ flies as compared with controls expressing GFP. In addition, we used a flight assay to measure the flying ability of 128Qhtt$^{FL}$ flies. Flying ability is determined as a function of flight distance after flies are dropped from the top of a transparent cylinder (Pesah et al., 2004). We found that 25-day-old 128Qhtt$^{FL}$ flies exhibit a severe flight-impairment phenotype, while GFP control and 16Qhtt$^{FL}$ flies of the same age behave normally (Figure 3C).

To substantiate a correlation between neurodegeneration and flight impairments in the 128Qhtt$^{FL}$-expressing flies, we investigated the neuronal projections into the Indirect Flight Muscles (IFM). Labeling of the motor neurons innervating the IFM shows a neurodegenerative phenotype in aged 128Qhtt$^{FL}$ flies, but not 16Qhtt$^{FL}$ control flies of the same age (Figures 3D and 3E,

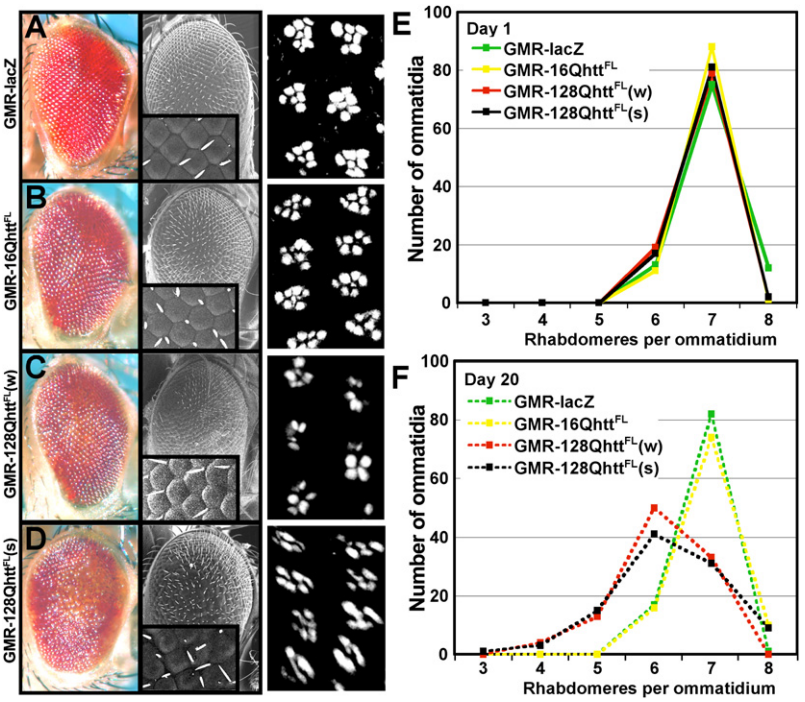


**Figure 2. Progressive Neurodegenerative Eye Phenotype Produced by Overexpression of Expanded (128Q), but Not Unexpanded (16Q), Full-Length htt**

(A–D) Light microscope (left) and SEM (center) images of transgenic flies expressing (A) nontoxic LacZ control protein, (B) wild-type htt, (C) low levels of expanded htt, and (D) high levels of expanded htt. Insets in SEM images show magnification (600×) of ommatidia. Note disorganization of ommatidia in (D). Right panels show phalloidin staining of the corresponding eyes from 20-day-old flies showing arrangement of rhabdomeres. Flies for light microscope and SEM images were raised at 25°C. Flies for phalloidin staining were raised at 27°C. Genotypes for light microscope and SEM: GMR-lacZ (*GMR-GAL4(s)/UAS-lacZ*), GMR-16Qhtt$^{FL}$ (*GMR-GAL4(s)/UAS-16Qhtt$^{FL}$[M28]*), GMR-128Qhtt$^{FL}$(w) (*GMR-GAL4(s)/+; UAS-128Qhtt$^{FL}$(w)[F7]/+*), GMR-128Qhtt$^{FL}$ (*GMR-GAL4(s)/UAS-128Qhtt$^{FL}$(s)[M36E2]*). Genotypes for phalloidin staining: GMR-lacZ (*GMR-GAL4/UAS-lacZ*), GMR-16Qhtt$^{FL}$ (*GMR-GAL4/UAS-16Qhtt$^{FL}$[M28]*), GMR-128Qhtt$^{FL}$ (*GMR-GAL4/+; UAS-128Qhtt$^{FL}$(w)[F7]*), GMR-128Qhtt$^{FL}$ (*GMR-GAL4/UAS-128Qhtt$^{FL}$[M36E2]*).

(E and F) Quantification of the number of rhabdomeres per ommatidium in 1-day-old (E) or 20-day-old (F) flies expressing the following proteins. Green, nontoxic LacZ control; yellow, wild-type htt; red, expanded htt at relatively low levels; black, expanded htt at relatively high levels. Flies raised at 27°C. n = 100 ommatidia per genotype. The distribution of the rhabdomeres at day 20 for 128Qhtt$^{FL}$(w) and 128Qhtt$^{FL}$(s) is significantly different from LacZ and 16Qhtt$^{FL}$ controls ($p < 0.001$, Mann-Whitney test). Genotypes: GMR-lacZ (*GMR-GAL4/UAS-lacZ*), GMR-16Qhtt$^{FL}$ (*GMR-GAL4/UAS-16Qhtt$^{FL}$[M28]*), GMR-128Qhtt$^{FL}$(w) (*GMR-GAL4/+; UAS-128Qhtt$^{FL}$(w)[F7]*), GMR-128Qhtt$^{FL}$(s) (*GMR-GAL4/UAS-128Qhtt$^{FL}$(s)[M36E2]*).

$p < 0.05$, Mann-Whitney test). Together, these data indicate that expression of expanded full-length htt causes progressive degenerative phenotypes in PNS and CNS neurons in *Drosophila*.

## Htt Is Unevenly Distributed across Synaptic Boutons, but Does Not Affect the Distribution of Key Synaptic Proteins

We investigated the mechanism by which 128Qhtt$^{FL}$ triggers the eye and CNS phenotypes described above. Potentially important mechanisms of pathogenesis in HD are transcriptional dysregulation (Sugars and Rubinsztein, 2003), impaired axonal transport (Gunawardena and Goldstein, 2005; Li and Li, 2004a), synaptic dysfunction (Smith et al., 2005), and abnormal $Ca^{2+}$ homeostasis (Bezprozvanny and Hayden, 2004). Because we did not detect 128Qhtt$^{FL}$ nuclear accumulation or axonal aggregation of 128Qhtt$^{FL}$ or synaptotagmin, we focused on synaptic dysfunction and $Ca^{2+}$ homeostasis.

First we studied the distribution of full-length htt in synaptic terminals. Interestingly, htt, driven by the Elav-GAL4 panneural driver exhibits a nonuniform distribution across boutons within a single third-instar larval neuromuscular junction (NMJ) (Figure 4A). We also studied the distribution of proteins involved in synaptic transmission in 128Qhtt$^{FL}$ and control animals. Figure 4B shows that soluble NSF-attachment protein, Snap (Ordway et al., 1994), Ras opposite (Rop) (Schulze et al., 1994), and syntaxin 1A (Syx) (Schulze et al., 1995) are normally distributed in boutons expressing 128Qhtt$^{FL}$. Also, we did not observe noticeable abnormalities in bouton number, branching, or morphology in 128Qhtt$^{FL}$ larvae (data not shown). In 128Qhtt$^{FL}$ flies, htt is expressed in the presynaptic neurons and is not present in the postsynaptic muscles. Therefore, we do not expect significant changes in postsynaptic glutamate receptor clusters. Nonetheless, to visualize neurotransmitter receptor clusters at the NMJ, we labeled 128Qhtt$^{FL}$ and 16Qhtt$^{FL}$ control flies with GluRIIA antibodies (Schuster et al., 1991). Receptor cluster abundance is not significantly different in 128Qhtt$^{FL}$ and 16Qhtt$^{FL}$ animals (Figure 4B, uppermost row panels, $p > 0.5$, Mann-Whitney test). Hence, postsynaptic neurotransmitter receptor clustering appears unaffected by neuronal expression of expanded full-length htt. These observations suggest that abnormal bouton morphology, altered synaptic protein accumulation, or both together are not responsible for the eye and CNS phenotypes observed in 128Qhtt$^{FL}$ flies.

## Increased Neurotransmitter Release Probability upon Expression of 128Qhtt$^{FL}$

Because the immunolabeling studies of the NMJ using confocal microscopy did not reveal major differences in abundance or distribution of synaptic proteins between 128Qhtt$^{FL}$ and control animals, we investigated possible electrophysiological defects. To determine the properties of neurotransmitter release in neurons expressing 128Qhtt$^{FL}$ presynaptically, we recorded excitatory junctional potentials (EJPs) at the third-instar larval NMJ. Although EJPs recorded from animals expressing either 128Qhtt$^{FL}$ or GFP in the nervous system (Elav-128Qhtt$^{FL}$ or Elav-GFP, respectively) are similar at 1.2 mM extracellular $Ca^{2+}$ (Elav-GFP:

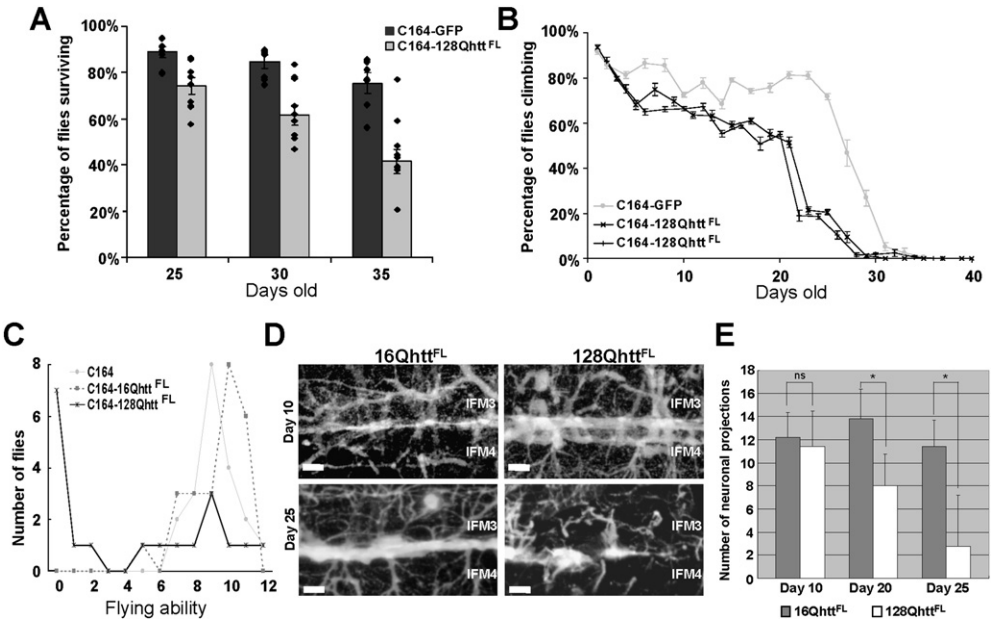


**Figure 3. Reduced Survival, Impaired Motor Performance, and Neuronal Degeneration in *Drosophila* Expressing Expanded Full-Length htt in the CNS**

(A) Average survival of flies expressing GFP (dark bars) or 128Qhtt$^{FL}$ (light bars) in the CNS (C164-GAL4) at days 25, 30, and 35. The survival rate of flies expressing 128Qhtt$^{FL}$ is significantly lower than the survival rate of control flies expressing a nontoxic GFP protein ($p < 0.05$, $p < 0.01$, and $p < 0.01$, respectively, Mann-Whitney test). Dots denote single data points for individual populations. Error bars = SEM; n = 7 and 10 populations for GFP and 128Qhtt$^{FL}$, respectively.

(B) Climbing performance as a function of age in control and 128Qhtt$^{FL}$-expressing flies. Normal decline in climbing performance is observed after day 25 in flies expressing the nontoxic GFP protein (silver line). In contrast, flies expressing 128Qhtt$^{FL}$ (black lines) perform poorly after day 20. All flies raised at 27°C. Two independent experiments are shown for flies expressing 128Qhtt$^{FL}$. Error bars = SEM of ten trials per time point.

(C) Flying ability in 25-day-old control and htt-expressing flies. Flying ability is represented in arbitrary units, with 12 being a perfect ability and 0 being no ability. Note that most control flies that carry only the motor neuron driver (silver line) or express wild-type htt (16Qhtt$^{FL}$, gray dotted lines) perform well in this assay, with no significant difference between them ($p > 0.1$, Mann-Whitney test). Most flies expressing expanded htt (128Qhtt$^{FL}$, black lines), on the other hand, show impaired flying ability when compared to either control ($p < 0.05$, Mann-Whitney test).

(D) Stacks of confocal images of neurons projecting into indirect flight muscles (IFM) 3 and 4 of 10-day (upper panels) and 25-day (lower panels) -old flies expressing wild-type (left) or expanded (right) htt. Note the loss of neuronal projections and NMJs in flies expressing expanded htt. Scale bar, 10 μm.

(E) Quantification of the number of neuronal projections in a specified 100 μm × 100 μm area of IFM 3/4 shown in (D). 20-day and 25-day, but not 10-day old flies expressing 128Qhtt$^{FL}$ have significantly fewer neuronal projections than control flies of the same age expressing wild-type 16Qhtt$^{FL}$ protein (ns: $p > 0,05$; *$p < 0.05$, Student's t test; n = 5).

All flies raised at 27°C. Genotypes: C164 (*C164-GAL4/+*), C164-GFP (*C164-GAL4/UAS-GFP),* C164-16Qhtt$^{FL}$ (*C164-GAL4/UAS-16Qhtt$^{FL}$[M28]*), C164-128Qhtt$^{FL}$ (*C164-GAL4/UAS-128Qhtt$^{FL}$(s)[M36E2]*).

40.5 ± 2.0 mV; Elav-128Qhtt$^{FL}$: 44.2 ± 0.6 mV; t test, $p > 0.1$, data not shown), EJPs recorded at lower extracellular $Ca^{2+}$ are clearly different. As shown in Figures 5A–5C, EJPs recorded from Elav-128Qhtt$^{FL}$ animals in 0.25 mM $Ca^{2+}$ are increased about 5-fold compared with those of Elav-GFP controls (Elav-GFP: 2.9 ± 0.3 mV; Elav-128Qhtt$^{FL}$: 16.0 ± 2.7 mV; t test, $p < 0.001$), whereas EJPs recorded in 0.6 mM $Ca^{2+}$ are increased by ~30% (Elav-GFP: 27.7 ± 3.0 mV; Elav-128Qhtt$^{FL}$: 36.3 ± 2.4 mV; t test, $p < 0.05$). The increased neurotransmission is specific to expression of 128Qhtt$^{FL}$ because expression of wild-type 16Qhtt$^{FL}$ does not produce this effect (Figures 5B and 5C; Elav-16Qhtt$^{FL}$ in 0.25 mM $Ca^{2+}$: 3.6 ± 0.8 mV; t test, $p > 0.7$). This phenotype is not simply an effect of the 128Qhtt$^{FL}$ transgene insertion site because flies carrying the transgene in the absence of the Elav driver do not differ from GFP controls (128Qhtt$^{FL}$: 3.08 ± 0.63 mV; Elav-GFP: 2.9 ± 0.3 mV). Thus, expression of expanded htt protein in neurons leads to increased synaptic transmission at the NMJ of third-instar *Drosophila* larvae.

Because our data argue against abnormal glutamate receptor clustering (see above), the increased synaptic transmission in 128Qhtt$^{FL}$ animals could be caused by increased neurotransmitter release from individual synaptic vesicles or increased release efficiency. To test whether neurotransmitter release from single vesicles is altered in Elav-128Qhtt$^{FL}$ animals, we recorded spontaneous fusion events in the absence of stimulation (mEJPs or minis; 0.1 mM $Ca^{2+}$ and 5 M TTX). As shown in Figures 5D and 5E, mEJP frequency and amplitude are similar in Elav-128Qhtt$^{FL}$ and Elav-GFP animals, indicating that transmitter loading and postsynaptic glutamate receptor clustering are unaffected.

Finally, to determine release probability, we recorded the number of failures (nonevents) when motor neurons were stimulated two to three times above threshold in low (0.25 mM) $Ca^{2+}$. Interestingly, whereas controls (Elav-GFP, Elav-16Qhtt$^{FL}$, and 128Qhtt$^{FL}$ with no driver) fail to release about 20%–25% of the time (Figure 5F), animals that express 128Qhtt$^{FL}$ reliably release neurotransmitter upon stimulation, with very low failure rates

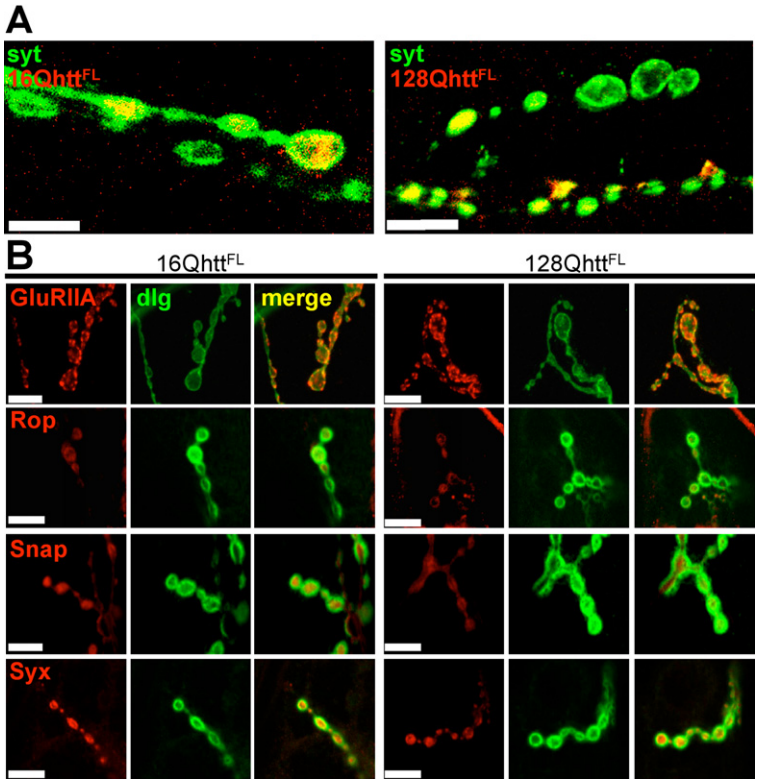


**Figure 4. Uneven Distribution of Full-Length htt across Boutons Does Not Affect Distribution of Key Synaptic Proteins**

(A) Immunofluorescence confocal images of NMJs from third-instar larvae expressing wild-type (left) or expanded (right) htt reveal its uneven distribution from one bouton to another within individual axons. Boutons are visualized with anti-synaptotagmin antibody (green), and htt is labeled in red. Scale bar, 10 μm.

(B) Immunofluorescence confocal images of NMJs from third-instar larvae expressing wild-type (left) or expanded (right) htt show morphologically normal boutons with no abnormal distribution of proteins involved in neurotransmitter secretion. Boutons are visualized with anti-dlg (green) and stained for (from top to bottom) GluRIIA, Rop, Snap, and Syx (red). No differences are detected in the patterns of accumulation of any of these proteins in boutons from larvae expressing expanded htt or boutons from control larvae expressing wild-type htt ($p > 0.5$, $p > 0.1$, $p > 0.1$, and $p > 0.1$, respectively). Scale bar, 5 μm. All larvae raised at 29°C. Genotypes: 16Qhtt$^{FL}$ (*Elav-GAL4/+; UAS-16QhttFL(s)[M28]/+*), 128Qhtt$^{FL}$ (*Elav-GAL4/+; UAS-128QhttFL(s)[M36E2]/+*).

(0.3% ± 0.3% failures; t test, $p < 0.001$). Hence, the increased synaptic transmission observed in animals that express 128Qhtt$^{FL}$ is, at least in part, caused by an increase in neurotransmitter release probability.

## Partial Loss of Function of Genes Required for Proper Synaptic Transmission Suppresses Neurotransmitter Release Abnormalities Caused by 128Qhtt$^{FL}$

Because expression of 128Qhtt$^{FL}$ causes increased synaptic transmission and release probability, an attractive possibility is that reducing the activity of components of the neurotransmitter release machinery may ameliorate these phenotypes, providing a potential therapeutic strategy.

To test this hypothesis, we recorded EJP amplitudes in 0.25 mM $Ca^{2+}$ and determined the release probability in 128Qhtt$^{FL}$ flies that lack one functional copy of Soluble NSF attachment protein (Snap), syntaxin1A (Syx), or proteins that are known to bind Syx, like Rop (Schulze et al., 1994) and Vha100-1 (Hiesinger et al., 2005). Syx is a plasma membrane-associated member of the SNARE complex that mediates fusion between the vesicular and synaptic membranes (Schulze et al., 1995). Snap associates with the SNARE complex and assists N-ethylmaleimide Sensitive Fusion Protein (NSF) in the dissociation of SNARE complexes (Ordway et al., 1994). Rop, the *Drosophila* Sec1 homolog, interacts with syntaxin in vivo and has both positive and inhibitory functions on neurotransmission (Wu et al., 1998). Whereas animals that overexpress 128Qhtt$^{FL}$ in the nervous system show increased EJP amplitude and decreased failure rate (Figure 5B and 5F), removing one copy of Snap (*Elav-GAL4/+; UAS-128Qhtt$^{FL}$(s)[M36E2]/+; Snap$^{M4}$/+*) suppresses these phenotypes and restores the EJP amplitude and failure rates to control levels (Figures 6A, 6B, 6I, and 6L). This suppression effect is not a result of reduced transmission in animals that have lost one copy of Snap, because the EJP amplitude and failure rates in *Elav-GAL4/+; Snap$^{M4}$/+* larvae are not different from controls (*Elav-GAL4/+;* UAS-GFP/+) (Figures 6A, 6B, 6J, and 6K). Similarly, although removing one copy of Rop (*Elav-GAL4/+; Rop$^{G27}$/+*) (Figures 6C, 6D, 6M, and 6N) or one copy of Syx (*Elav-GAL4/+; Syx$^{229}$/+*) (Figures 6E and 6F) does not affect EJP amplitudes or failure rates compared with controls at 0.25 mM $Ca^{2+}$, it efficiently suppresses the increased EJP amplitude and decreased failure rates observed in Elav-128Qhtt$^{FL}$ animals.

Not all components of the release machinery are able to suppress the increased release in Elav-128Qhtt$^{FL}$ larvae to the same extent. The Vha100-1 subunit is an important component of the synaptic vesicle release machinery, recently shown to act downstream of the SNARE complex in neurons (Hiesinger et al., 2005). Removing one copy of *Vha100-1* in 128Qhtt$^{FL}$-expressing animals (*Elav-GAL4/+; UAS-128Qhtt$^{FL}$(s)[M36E2]/+; vha$^{1}$/+*) does not fully suppress the increased EJP amplitude seen in Elav-128Qhtt$^{FL}$ larvae and fails to suppress the increased release probability (Figures 6G and 6H). Taken together, these data suggest that neuronal expression of expanded htt facilitates neurotransmitter release by acting upon a general process that promotes vesicle release.

## Synaptic Transmission Mutations Also Suppress the Eye Neurodegeneration and Motor Performance Phenotypes Caused by 128Qhtt$^{FL}$

If increased neurotransmitter release is an important mechanism by which expanded full-length htt exerts its toxicity on 128Qhtt$^{FL}$ flies, one may expect that suppressors of the electrophysiological phenotype also suppress other defects observed in these

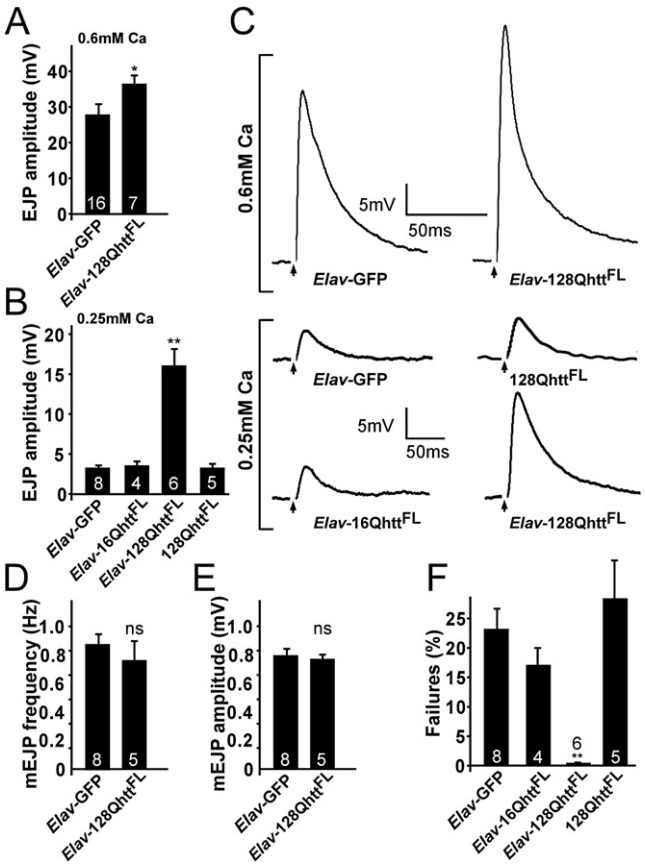


**Figure 5. Neurotransmitter Release Probability Is Increased upon Expression of Full-Length Expanded htt**

(A and B) Quantification of EJP amplitudes recorded at (A) 1 Hz in 0.6 mM $Ca^{2+}$ or (B) 0.25 mM $Ca^{2+}$ in *Drosophila* larvae expressing a nontoxic control protein (GFP), wild-type, or expanded full-length htt or controls carrying the htt transgene without a GAL4 driver. ns: $p > 0.05$; *$p < 0.05$; **$p < 0.01$ throughout the figure.

(C) Sample EJP traces recorded from *Drosophila* larvae expressing GFP control protein and expanded full-length htt in HL3 buffer at 0.6 mM $Ca^{2+}$ (top) or 0.25 mM $Ca^{2+}$ (bottom). For 0.25 mM $Ca^{2+}$, sample traces are also shown for transgenic larvae expressing wild-type htt and for controls carrying the expanded htt transgene without a GAL4 driver. Arrows indicate blanked-out stimulus artifact.

(D and E) Average (D) frequency and (E) amplitude of mEJPs recorded from abdominal muscle 6 or 7 in GFP control and larvae expressing expanded htt. Error bars = SEM. Number inside bars is the number of animals studied.

(F) Percent failures measured at 1 Hz in 0.25 mM $Ca^{2+}$ following stimulation at two to three times threshold of motor neurons in larvae expressing a nontoxic GFP protein, wild-type htt, expanded htt or controls carrying the htt transgene without a GAL4 driver. All experiments done at 29°C. Genotypes: *Elav-GFP* (*Elav-GAL4/+; UAS-GFP/+*), *Elav-16Qhtt$^{FL}$* (*Elav-GAL4/+; UAS-16Qhtt$^{FL}$[M28]/+*), *128Qhtt$^{FL}$* (*UAS-128Qhtt$^{FL}$(s)[M36E2]/+*), *Elav-128Qhtt$^{FL}$* (*Elav-GAL4/+; UAS-128Qhtt$^{FL}$(s)[M36E2]/+*).

animals. To test this hypothesis, we assessed the ability of neurotransmitter release mutations to suppress the degenerative phenotype observed in eye photoreceptors of 128Qhtt$^{FL}$ flies. At 20 days, flies expressing 128Qhtt$^{FL}$ (*GMR-GAL4/+; UAS-128Qhtt$^{FL}$(w)[F7]/+*) show fewer rhabdomeres per ommatidium than controls (*GMR-GAL4/UAS-GFP*) (Figures 2F, 7A, and 7B). However, animals expressing 128Qhtt$^{FL}$ in the context of reduced function of *Snap* (*GMR-GAL4/+; UAS-128Qhtt$^{FL}$(w)[F7]/Snap$^{M4}$*) show a reversal of this neurodegenerative phenotype (Figures 7A and 7C, $p < 0.001$, Mann-Whitney test). Similar results were also obtained with animals having only one functional copy of the *Syntaxin 1A* gene (*GMR-GAL4/+; UAS-128Qhtt$^{FL}$(w)[F7]/Syx$^{229}$*, Figures 7A and 7D, $p < 0.001$, Mann-Whitney test) or the *Rop* gene (*GMR-GAL4/+; UAS-128Qhtt$^{FL}$(w)[F7]/Rop$^{G27}$*, Figures 7A and 7E, $p < 0.001$, Mann-Whitney test). Partial loss of function of Vha100-1, on the other hand, did not improve the eye degeneration (*GMR-GAL4/+; UAS-128Qhtt$^{FL}$(w)[F7]/vha $^{1}$*, Figures 7A and 7G, $p > 0.5$, Mann-Whitney test). Moreover, we observed suppression of the 128Qhtt$^{FL}$ external eye phenotype with reduced activity of the neurotransmitter release gene *Syx* (Figures 7J–7L). These data indicate a link between increased neurotransmission and neuronal degeneration in 128Qhtt$^{FL}$ animals.

In addition to the eye assay, we tested the ability of one mutant copy of *Syx* to suppress the motor performance defects caused by expression of 128Qhtt$^{FL}$ in the CNS. Flies expressing 128Qhtt$^{FL}$ (*C164-GAL4/+; UAS-128Qhtt$^{FL}$(s)[M36E2]/+*) perform poorly in the climbing assay relative to controls, but this phenotype is suppressed in 128Qhtt$^{FL}$ flies that are heterozygous mutant for *Syx* (*C164-GAL4/+; UAS-128Qhtt$^{FL}$(s)[M36E2]/+; Syx$^{229}$/+*; see Figure 7I). These results validate the fact that loss-of-function mutations in components of the neurotransmitter release machinery act as suppressors in different assays, and they underscore the importance of synaptic transmission dysfunction in 128Qhtt$^{FL}$-induced neurodegeneration.

## Increased $Ca^{2+}$ Levels in Synaptic Terminals of *Drosophila* Expressing 128Qhtt$^{FL}$ Are Restored by Mutations in Components of the Neurotransmitter Release Machinery

Intracellular $Ca^{2+}$ levels are elevated in lymphoblasts of HD mouse models, and expanded htt has been shown to potentiate NMDAR (NR1/NR2B)-induced apoptosis and $Ca^{2+}$ transients (Cepeda et al., 2001; Hodgson et al., 1999; Tang et al., 2005). Hence, we investigated whether elevated presynaptic $Ca^{2+}$ levels may account for increased vesicle release at 128Qhtt$^{FL}$ synapses by measuring presynaptic $Ca^{2+}$ levels at the NMJ of 128Qhtt$^{FL}$ third-instar larvae. To assess resting intracellular $Ca^{2+}$ levels at presynaptic terminals, we forward-filled motor axons of control and 128Qhtt$^{FL}$ larvae with the ratiometric dye Fura-2 Dextran. Upon $Ca^{2+}$ binding, the maximal excitation of Fura-2 shifts from ~380 nm to ~340 nm. Therefore, the fluorescence ratio, $F_{340}/F_{380}$, provides a relative measure of $Ca^{2+}$ levels. We found that resting synaptic $Ca^{2+}$ levels are elevated on average by ~2-fold in 128Qhtt$^{FL}$ larvae compared with GFP controls. A similar effect was also found in 16Qhtt$^{FL}$ larvae (Figure 8A). In addition, $Ca^{2+}$ levels are more variable at 128Qhtt$^{FL}$ synapses compared with those of GFP controls (f test, $p < 0.001$), with a bimodal distribution of fluorescence ratios indicative of bouton populations with both normal and aberrant intracellular $Ca^{2+}$ levels (Figure 8A; open diamonds denote individual data points). This observation concurs with the uneven distribution of 128Qhtt$^{FL}$ in synaptic boutons described above (Figure 4A).

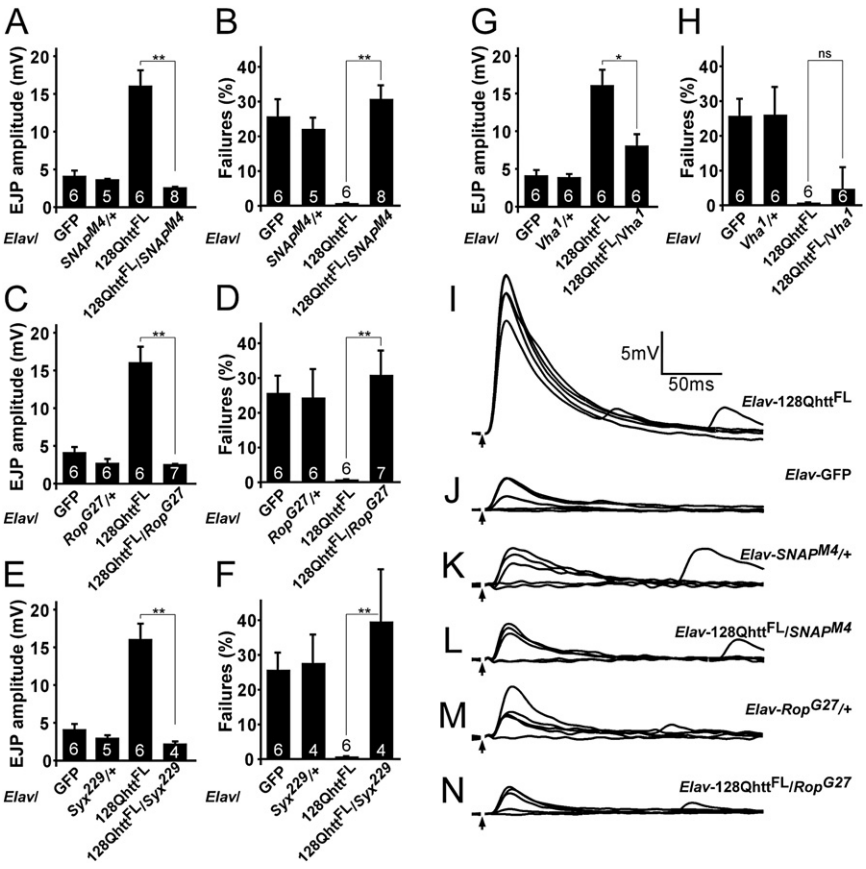


**Figure 6. Heterozygous Mutations in Genes Affecting Secretion Suppress the Increased Release Probability Caused by Full-Length Expanded htt**

(A–H) Quantification of EJP amplitudes (A, C, E, and G) and percent failures (B, D, F, and H) in larvae expressing a nontoxic control protein GFP, heterozygous mutant for (A and B) Snap, (C and D) Rop, (E and F) syntaxin 1A, or (G and H) Vha100kDa, expressing expanded htt or expressing expanded htt as well as heterozygous mutant for either (A and B) Snap, (C and D) Rop, (E and F) syntaxin 1A, or (G and H) Vha100-1 at 29°C. Error bars = SEM. Number inside bars is the number of animals studied. ns, $p > 0.05$; *$p < 0.05$; **$p < 0.01$. Experiments done at 29°C.

(I–N) Sample EJP traces (five consecutive traces recorded at 1 Hz interval) recorded from (I) larvae expressing expanded htt, (J) the control protein, GFP, (K) heterozygous mutant for Snap, (L) expressing expanded htt and heterozygous mutant for Snap, (M) heterozygous mutant for Rop and (N) expressing expanded htt and heterozygous mutant for Rop. Arrows indicate blanked-out stimulus artifact. All experiments done at 29°C. All recordings at 1 Hz in HL3 buffer at 0.25 mM $Ca^{2+}$. Genotypes: GFP (*Elav-GAL4/+; UAS-GFP/+*), $128Qhtt^{FL}$ (*Elav-GAL4/+; UAS-128Qhtt$^{FL}$(s)[M36E2]/+*), *Snap$^{M4}$/+* (*Elav-GAL4/+; Snap$^{M4}$/+*), $128Qhtt^{FL}$/*Snap$^{M4}$* (*Elav-GAL4/+; UAS-128Qhtt$^{FL}$(s)[M36E2]/+; Snap$^{M4}$/+*), *Rop$^{27}$/+* (*Elav-GAL4/+; Rop$^{G27}$/+*), $128Qhtt^{FL}$/*Rop$^{G27}$* (*Elav-Gal4/+; UAS-128Qhtt$^{FL}$(s)[M36E2]/+; Rop$^{G27}$/+*), *Syx$^{229}$/+* (*Elav-GAL4/+; Syx$^{229}$/+*), $128Qhtt^{FL}$/*Syx$^{229}$* (*Elav-Gal4/+; UAS-128Qhtt$^{FL}$(s)[M36E2]/+; Syx$^{229}$/+*), *vha$^{1}$/+* (*Elav-GAL4/+; vha$^{1}$/+*), $128Qhtt^{FL}$/*vha$^{1}$* (*Elav-GAL4/+; UAS-128Qhtt$^{FL}$(s)[M36E2]/+; vha$^{1}$/+*).

In order to mediate efficient release, vesicles are positioned closely to sites of $Ca^{2+}$ influx via interactions between presynaptic release proteins, including syntaxin, SNAP-25, and the synprint region of voltage-gated $Ca^{2+}$ channels (Katz and Miledi, 1965; Swayne et al., 2005). Htt interacts with subunits of voltage-gated $Ca^{2+}$ channels present at the synapse and may functionally alter $Ca^{2+}$ channel function (Swayne et al., 2005). These data suggest that, while interactions of expanded htt may interfere with components of the release machinery, they may also disturb $Ca^{2+}$ homeostasis at the synapses, resulting in increased neurotransmitter release.

To investigate whether the elevated presynaptic $Ca^{2+}$ levels stem from interactions between expanded htt and the synaptic release machinery, we determined resting $Ca^{2+}$ levels in larvae overexpressing $128Qhtt^{FL}$ but lacking one functional copy of *Syx*. Compared with animals expressing $128Qhtt^{FL}$ alone, which have elevated synaptic $Ca^{2+}$ levels (Figures 8A and 8B, *Elav-GAL4/+; UAS-128Qhtt$^{FL}$(s)[M36E2]/+*: $F_{340}/F_{380} = 0.83 \pm 0.42$), $128Qhtt^{FL}$ animals with only one functional copy of *Syx* exhibit a reduction in $Ca^{2+}$ (Figures 8A and 8B, *Elav-GAL4/+; UAS-128Qhtt$^{FL}$(s)[M36E2]/+; Syx$^{229}$/+*: $F_{340}/F_{380} = 0.39 \pm 0.07$) and show levels similar to those of controls (Figures 8A and 8B, *Elav-GAL4/+; UAS-GFP/+*: $F_{340}/F_{380} = 0.28 \pm 0.04$). Because voltage-gated $Ca^{2+}$ channels are critical purveyors of presynaptic calcium entry and synaptic release, we investigated whether reduced calcium channel activity also corrects the $128Qhtt^{FL}$-induced elevation in calcium levels. Two *Drosophila* voltage-gated $Ca^{2+}$ channel pore subunits are expressed in neurons (Kawasaki et al., 2000; Zheng et al., 1995). Dmca1D is an L-type voltage-gated $Ca^{2+}$ channel, while Dmca1A, also known as cacophony, is a P/Q-type voltage-gated channel; both mediate $Ca^{2+}$ influx at the presynaptic terminal (Kawasaki et al., 2000; Zheng et al., 1995). Interestingly, the increased $Ca^{2+}$ levels are normalized in $128Qhtt^{FL}$-expressing animals with only one functional copy of *Dmca1D* (*Elav-GAL4/+; UAS-128Qhtt$^{FL}$(s)[M36E2]/Dmca1D$^{X10}$*: $F_{340}/F_{380} = 0.29 \pm 0.04$). This reduction is not due to the loss of either *Syx* or *Dmca1D* alone because *Elav-GAL4/+; Syx$^{229}$/+* and *Elav-GAL4/+; Dmca1D$^{X10}$/+* have similar resting $Ca^{2+}$ levels as controls (Figure 8A, *Elav-GAL4/+; Syx$^{229}$/+*: $F_{340}/F_{380} = 0.30 \pm 0.05$; *Elav-GAL4/+; Dmca1D$^{X10}$/+*: $F_{340}/F_{380} = 0.24 \pm 0.05$). Because $Ca^{2+}$ is required upstream of vesicle fusion, this suggests that alterations in neurotransmission at synapses that accumulate $128Qhtt^{FL}$ may stem from an elevation in synaptic $Ca^{2+}$ levels. In addition, interactions between $128Qhtt^{FL}$ and the vesicle release machinery may serve to modulate synaptic efficacy by regulating synaptic $Ca^{2+}$ levels.

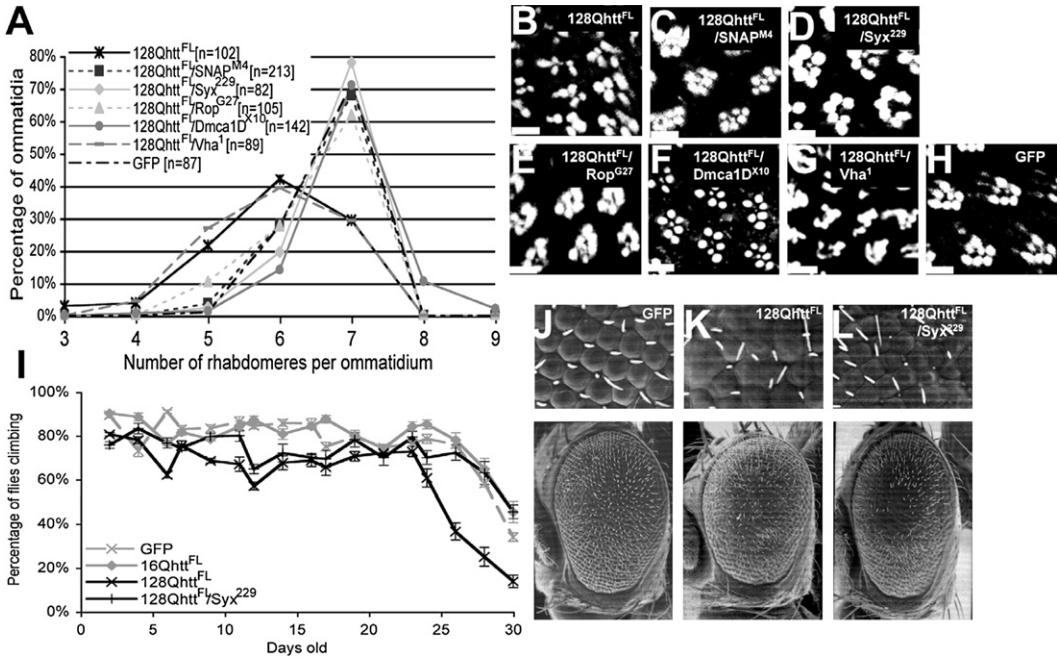


**Figure 7. Heterozygous Mutations in Genes Affecting Neurotransmitter Secretion also Suppress Neurodegeneration and Motor Impairments in Animals Expressing Expanded Full-Length htt**

(A) Number of rhabdomeres per ommatidium in 20-day-old flies of the indicated genotypes. The distribution of the rhabdomeres is significantly different ($p < 0.001$, Mann-Whitney test) between 128Qhtt$^{FL}$ and 128Qhtt$^{FL}$ animals also carrying one mutant copy of SNAP, Syx, Rop, or Dmca1D. Flies grown at 27°C. Genotypes: 128Qhtt$^{FL}$ (*GMR-GAL4/+; UAS-128Qhtt$^{FL}$(w)[F7]*), 128Qhtt$^{FL}$/*Snap$^{M4}$* (*GMR-GAL4/+; UAS-128Qhtt$^{FL}$(w)[F7]/Snap$^{M4}$*), 128Qhtt$^{FL}$/*Syx$^{229}$* (*GMR-GAL4/+; UAS-128Qhtt$^{FL}$(w)[F7]/Syx$^{229}$*), 128Qhtt$^{FL}$/*Rop$^{G27}$* (*GMR-GAL4/+; UAS-128Qhtt$^{FL}$(w)[F7]/Rop$^{G27}$*), 128Qhtt$^{FL}$/*Dmca1D$^{X10}$* (*GMR-GAL4/ Dmca1D$^{X10}$; UAS-128Qhtt$^{FL}$(w)[F7]/+*), 128Qhtt$^{FL}$/*vha$^{1}$* (*GMR-GAL4/+; UAS-128Qhtt$^{FL}$(w)[F7]/vha$^{1}$*), GFP (*GMR-GAL4/ UAS-GFP*).

(B–H) Phalloidin staining of dissected retinas from 20-day-old flies of the genotypes indicated in each panel. Scale bar, 5 μM. Flies grown at 27°C. Genotypes: (B), 128Qhtt$^{FL}$ (*GMR-GAL4/+; UAS-128Qhtt$^{FL}$(w)[F7]/+*); (C), 128Qhtt$^{FL}$/Snap$^{M4}$ (*GMR-GAL4/+; UAS-128Qhtt$^{FL}$(w)[F7]/Snap$^{M4}$*); (D), 128Qhtt$^{FL}$/*Syx$^{229}$* (*GMR-GAL4/+; UAS-128Qhtt$^{FL}$(w)[F7]/Syx$^{229}$*); (E), 128Qhtt$^{FL}$/*Rop$^{G27}$* (*GMR-GAL4/+; UAS-128Qhtt$^{FL}$(w)[F7]/Rop$^{G27}$*); (F), 128Qhtt$^{FL}$/*Dmca1D$^{X10}$* (*GMR-GAL4/Dmca1D$^{X10}$; UAS-128Qhtt$^{FL}$(w)[F7]/+*); (G), 128Qhtt$^{FL}$/*Vha$^{1}$* (*GMR-GAL4/+; UAS-128Qhtt$^{FL}$(w)[F7]/Vha$^{1}$*); (H), GFP (*GMR-GAL4/UAS-GFP*).

(I) Suppression of climbing performance phenotype in flies expressing 128Qhtt$^{FL}$ and heterozygous for a loss-of-function mutation in *Syx*. Flies expressing the non-toxic GFP protein or 16Qhtt$^{FL}$ show normal decline in climbing performance with age. Climbing performance impairment occurs prematurely in flies expressing 128Qhtt$^{FL}$, but it is restored in a background heterozygous mutant for *Syx*. Error bars = SEM of ten trials per time point. Flies grown at 25°C. Genotypes: GFP (*C164-GAL4/UAS-GFP*), 16Qhtt$^{FL}$ (*C164-GAL4/UAS-16Qhtt$^{FL}$[M28]*), 128Qhtt$^{FL}$ (*C164-GAL4/UAS-128Qhtt$^{FL}$(s)[M36E2]*), 128Qhtt$^{FL}$/*Syx$^{229}$* (*C164-GAL4/UAS-128Qhtt$^{FL}$(s)[M36E2]; Syx$^{229}$/+*).

(J–L) SEM eye images of flies expressing (J) the non-toxic control protein GFP, (K) 128Qhtt$^{FL}$ (L) 128Qhtt$^{FL}$ and heterozygous mutant for *Syx*. Note partial suppression of the disorganized ommatidia phenotype in *Syx* heterozygous mutant animals. Genotypes: lacZ (*GMR-GAL4(s)/UAS-GFP*), 128Qhtt$^{FL}$ (*GMR-GAL4(s)/UAS-128Qhtt$^{FL}$(s)[M36E2]*), 128Qhtt$^{FL}$(w)/*Syx$^{229}$* (*GMR-GAL4(s)/UAS-128Qhtt$^{FL}$(s)[M36E2]/+; Syx$^{229}$/+*). Flies grown at 25°C.

### Increased Transmission, Decreased Failures, and Photoreceptor Degeneration in 128Qhtt$^{FL}$ Animals Are Restored by Reducing the Activity of Voltage-Gated $Ca^{2+}$ Channels

To test whether $Ca^{2+}$ levels are a cause of increased transmission and decreased failures in 128Qhtt$^{FL}$ animals, we recorded EJPs at 0.25 mM $Ca^{2+}$ in Elav-128Qhtt$^{FL}$ flies that lack one copy of *Dmca1D* or *Dmca1A* (Figures 8C and 8D). As shown in Figures 8C and 8D, although neither *Elav-GAL4; Dmca1D$^{x10}$*/+ nor *Elav-GAL4, Dmca1A$^{HC129}$* harbor differing EJP amplitudes or failure rates compared with controls (Elav-GFP), both the increased EJP amplitude and the decreased failures observed in Elav-128Qhtt$^{FL}$ animals are significantly suppressed by removing one copy of either *Dmca1D* or *Dmca1A*. Likewise, the photoreceptor degeneration observed in 128Qhtt$^{FL}$-expressing flies is suppressed by removing one copy of *Dmca1D* (Figures 7A and 7F; $p < 0.001$, Mann-Whitney test). These data further support the hypothesis that altered intracellular $Ca^{2+}$ levels in neurons that express expanded htt lead to increased release probability and neuronal degeneration.

## DISCUSSION

Here we develop a *Drosophila* model of HD to investigate the mechanisms by which expanded full-length human htt causes neuronal dysfunction and degeneration. Targeted expression of 128Qhtt$^{FL}$ causes neuronal degeneration (both in eye photoreceptors and in the CNS), motor performance impairments, reduced lifespan, and increased neurotransmitter release. Importantly, these abnormalities occur in the absence of detectable htt nuclear import or axonal blockages and are specific to 128Qhtt$^{FL}$, because expression of similar levels of wild-type 16Qhtt$^{FL}$ does not cause abnormal phenotypes.

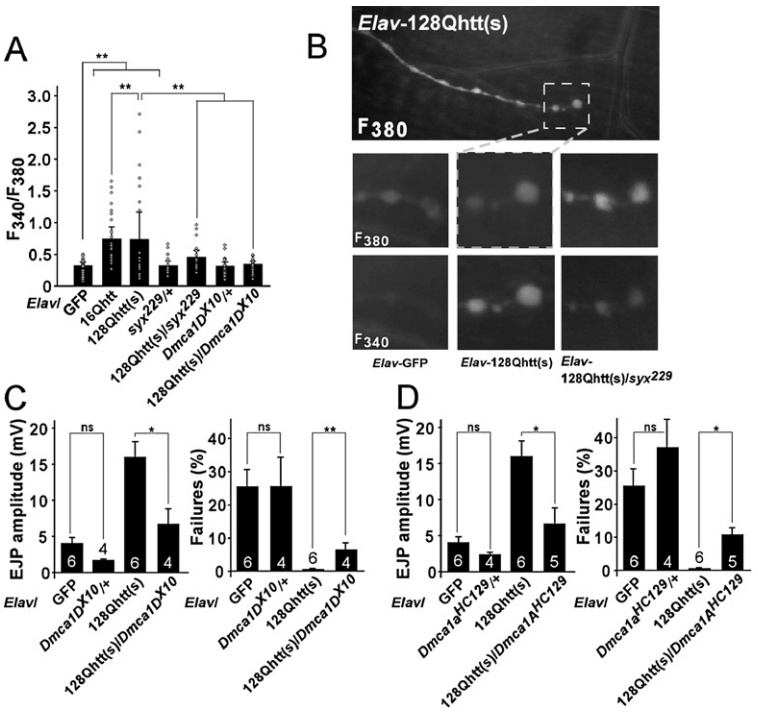


**Figure 8. Increased $Ca^{2+}$ Levels Caused by Expanded Full-Length htt Can Be Suppressed Genetically**

(A) Fluorescence ratios (F340/F380) measured from fura dextran-filled larval NMJs. Neuronal expression of 128Qhtt$^{FL}$ and 16Qhtt$^{FL}$ leads to increased fluorescence ratios compared to controls (GFP), indicating elevated resting $Ca^{2+}$ levels at these synapses (*$p < 0.05$, t test). These elevated fluorescence ratios are normalized in 128Qhtt$^{FL}$ animals that are also heterozygous for either *Syntaxin* or *Dmca1D* mutations (*$p < 0.05$, t test). Genotypes: *Elav-Gal4/+; UAS-128Qhtt$^{FL}$(s)[M36E2]/+; Syx$^{229}$/+* and *Elav-GAL4/+; UAS-128Qhtt$^{FL}$(s)[M36E2]/Dmca1D$^{X10}$*. Note that animals carrying *Syx* or *Dmca1D* heterozygous mutations but no htt transgene show no effect on resting $Ca^{2+}$ levels compared to GFP controls. Genotypes: *Elav-GAL4/+; Syx$^{229}$/+* and *Elav-GAL4/+; Dmca1D$^{X10}$/+*. Boutons were measured from two to three synapses in six larvae per genotype. Dots denote single data points from individual boutons.

(B) Fluorescence from boutons forward-filled with fura dextran and excited at both 340 nm and 380 nm. $Ca^{2+}$-free dye absorbs optimally at 380 nm while $Ca^{2+}$-bound dye is excited primarily at 340 nm. NMJ synapses loaded with fura dextran were clearly visualized (top panel) and individual boutons could be spatially resolved (dashed box). In contrast to controls (*Elav-GAL4/+; UAS-GFP/+*), NMJ boutons from larvae expressing expanded htt (*Elav-GAL4/+; UAS-128Qhtt$^{FL}$(s)[M36E2]/+*) emit more intensely when excited at 340 nm compared to 380 nm. However, *Syx* heterozygosity (*Elav-Gal4/+; UAS-128QhttFL(s)[M36E2]/+; Syx$^{229}$/+*) alleviates this phenotype.

(C and D) Quantification of EJP amplitudes and percent failures recorded at 1Hz in 0.25 mM $Ca^{2+}$ in larvae expressing a nontoxic GFP control protein, expressing 128Qhtt$^{FL}$, heterozygous mutant for *Dmca1D* (C), *Dmca1A* (D), or expressing 128Qhtt$^{FL}$ as well as heterozygous mutant for either *Dmca1D* (C) or *Dmca1A* (D). All experiments at done at 29°C. Error bars = SEM. The number of recordings from at least 3 animals is indicated inside the bars. ns, $p > 0.05$; *$p < 0.05$; **$p < 0.01$ throughout the figure. Genotypes: GFP (*Elav-GAL4/+; UAS-GFP/+*), 16Qhtt$^{FL}$ (*Elav-GAL4/+; UAS-16Qhtt$^{FL}$(s)[M28]/+*), 128Qhtt$^{FL}$ (*Elav-GAL4/+; UAS-128Qhtt$^{FL}$(s)[M36E2]/+*), *Syx$^{229}$/+* (*Elav-GAL4/+; Syx$^{229}$/+*), 128Qhtt$^{FL}$/*Syx$^{229}$* (*Elav-Gal4/+; UAS-128Qhtt$^{FL}$(s)[M36E2]/+; Syx$^{229}$/+*), *Dmca1D$^{X10}$/+* (*Elav-GAL4/+; Dmca1D$^{X10}$/+*), 128Qhtt$^{FL}$/*Dmca1D$^{X10}$* (*Elav-GAL4/+; UAS-128Qhtt$^{FL}$(s)[M36E2]/Dmca1D$^{X10}$*), *Dmca1A$^{HC129}$/+* (*Elav-GAL4/Dmca1A$^{HC129}$*), 128Qhtt$^{FL}$/*Dmca1A$^{HC129}$* (*Elav-GAL4/Dmca1A$^{HC129}$; UAS-128Qhtt$^{FL}$(s)[M36E2]/+*).

Expression of 128Qhtt$^{FL}$ in the eye using *GMR-GAL4* leads to progressive photoreceptor neuron degeneration. Histological examination of the internal eye structure in flies of different ages reveals that the number and arrangement of rhabdomeres in photoreceptor cells is relatively normal in 1-day-old flies (Figure 2E), but degeneration is evident at day 20 (Figure 2F). Expression of 128Qhtt$^{FL}$ in motor neurons leads to motor impairment phenotypes. The 128Qhtt$^{FL}$ animals perform as controls do in a climbing assay when they are young, but their motor performance declines prematurely as they age. Moreover, flying ability is impaired in aged 128Qhtt$^{FL}$ flies, and they also show progressive loss of NMJs at the IFM. In addition, these flies show a reduced survival rate when compared with controls (Figures 3A–3E).

These neurodegenerative phenotypes are not likely a consequence of transcriptional dysregulation, because they occur in the absence of obvious nuclear htt, even in aged flies. We also investigated the possibility that axonal blockages trigger the phenotypes observed in 128Qhtt$^{FL}$ flies; axonal blockages and impaired fast axonal transport have been reported following expression of polyglutamine tracts alone or in the context of other polypeptides (Gunawardena et al., 2003), including expanded htt (Lee et al., 2004). However, we did not detect htt or synaptotagmin accumulation in the axons of 128Qhtt$^{FL}$ flies, even though we could reproduce the observation of axonal blockages reported with an expanded htt fragment (Figures 1C and 1D). Despite the absence of visible htt or synaptotagmin aggregates, the possibility that intracellular transport is decreased cannot be excluded (Szebenyi et al., 2003; Gauthier et al., 2004). However, we did not observe mislocalization or aberrant distribution of known synaptic markers that rely on vesicular transport for their proper synaptic localization (Figure 4B).

All together, these data suggest that the presynaptic accumulation of 128Qhtt$^{FL}$ impairs the function of factors involved in neurotransmitter release. This hypothesis agrees with abundant data describing protein interactions between htt and components of the synaptic machinery (Smith et al., 2005) and with findings in R6/1 and R6/2 mouse models that suggested a role for altered neurotransmitter release as a potential mechanism of HD pathogenesis. In R6/2 mice, synapsin phosphorylation is partially defective (Lievens et al., 2002), and in R6/1 mice glutamate levels are reduced and aspartate and GABA are increased (Nicniocaill et al., 2001). Moreover, increased NMDA receptor activity has been reported in full-length HD mice (Cepeda et al., 2001; Zeron et al., 2002), leading to a postsynaptic increase in $Ca^{2+}$ influx and abnormal synaptic transmission. In addition, $Ca^{2+}$ levels were found to be increased by almost 2-fold in CA1 pyramidal neurons in full-length HD mice (Hodgson et al., 1999). However, no defects were observed in paired-pulse facilitation, which questions the biological relevance of this finding. In addition, mutant htt has been implicated in aberrant mitochondrial $Ca^{2+}$ buffering (Panov et al., 2005), and it also increases

the sensitivity of the inositol 1,4,5-triphosphate ($IP_3$) receptor to $IP_3$, causing enhanced $Ca^{2+}$ release following mGluR1/5 activation (Tang et al., 2003). These data suggest that cytosolic $Ca^{2+}$ levels play a role in HD pathogenesis (Bezprozvanny and Hayden, 2004).

To test whether expanded htt impairs the normal function of proteins involved in synaptic transmission, we used a genetic approach using the 128Qhtt$^{FL}$ animals. We found that partial loss of function of Snap, syntaxin, or Rop restores the increased EJP amplitude observed in 128Qhtt$^{FL}$ larvae to near-normal levels (Figures 6A, 6C, and 6E). Moreover, the lack of neurotransmitter release failures is also suppressed by these mutations (Figures 6B, 6D, and 6F). These observations suggest that neurodegeneration in 128Qhtt$^{FL}$ flies is caused by increased synaptic transmission. In agreement with this hypothesis, we found a progressive neurodegenerative phenotype in the NMJ of adult 128Qhtt$^{FL}$ animals (Figures 3D and 3E). Most importantly, further support for this hypothesis comes from the observation that the same synaptic transmission mutants that restore the EJP amplitude and release failure abnormalities also suppress motor impairment, photoreceptor degeneration, or both in 128Qhtt$^{FL}$ adult animals (Figure 7 and Figure S1, available online).

$Ca^{2+}$ levels have a bimodal distribution in 128Qhtt$^{FL}$ flies, with some boutons showing high $Ca^{2+}$ levels and other boutons within the same neuromuscular junction showing levels in the normal range (Figure 8A, note also that 16Qhtt$^{FL}$ flies show a similar effect). This distribution can be correlated with the accumulation pattern of htt, which is present in some boutons and absent in others within a given neuromuscular junction (Figure 4A). We tested the hypothesis that $Ca^{2+}$ levels are relevant for the increased transmission and decreased failures observed in 128Qhtt$^{FL}$ animals using mutations in voltage-gated $Ca^{2+}$ channels. We found that $Ca^{2+}$ levels are restored within normal range in 128Qhtt$^{FL}$ flies carrying heterozygous mutations in either *Syx* or the *Dmca1D* $Ca^{2+}$ channel (Figures 8A and 8B). Furthermore, heterozygous mutants for either the *Dmca1A* or *Dmca1D* $Ca^{2+}$ channels also show suppression of the increased transmission and decreased failure phenotypes (Figures 8C and 8D). We also tested Dmca1D in the context of the eye assay and found that its partial loss of function suppresses photoreceptor degeneration (Figures 7A and 7F). These data support the hypothesis that increased $Ca^{2+}$ levels play an important role in the observed increased transmission in neurons of 128Qhtt$^{FL}$ animals. Interestingly, mutations in $K^+$ channels cause neurodegeneration in flies (Fergestad et al., 2006) and in humans (Waters et al., 2006), further supporting the idea that the increased release is responsible, at least in part, for neuronal degeneration caused by expanded htt.

The findings described in this report unveil a mechanism of pathogenesis for expanded htt that does not require its nuclear accumulation in detectable amounts. The increased synaptic transmission phenotype exerted by full-length htt likely represents a mechanism of pathogenesis taking place at early stages of disease progression. In later stages, cleavage of htt would compound the toxic effects of the full-length protein with fast axonal transport impairments and transcriptional dysregulation caused by N-terminal fragments. These findings point to increased synaptic transmission as a therapeutic target with the potential of delaying HD onset and thus likely impacting disease progression. The genetic data showing suppression of the synaptic transmission and neurodegenerative phenotypes further define specific therapeutic targets and support the idea that $Ca^{2+}$ channel antagonists, and perhaps other inhibitors of neurotransmission, offer an attractive therapeutic option due to their specificity and wide usage.

## EXPERIMENTAL PROCEDURES

### Generation of Htt Constructs and Strains

The 128Qhtt$^{FL}$ cDNA was generated by replacing an N-terminal fragment of a 16Qhtt$^{FL}$ cDNA (provided by Dr. Tagle, NIH) with the corresponding 128Q N-terminal fragment (Kaltenbach et al., 2007). The constructs were subsequently cloned into the pUAST vector (Brand and Perrimon, 1993) and injected in the $y^1w^{118}$ strain by standard procedures. Four 128Qhtt$^{FL}$ and three 16Qhtt$^{FL}$ lines were generated. GMR and Elav-GAL4 drivers were obtained from the Bloomington Stock Center, GMR(s)-GAL4 from Dr. P. Jin (Emory Univ. School Med.), C164-GAL4 from Dr. V. Budnik, (Univ. Massachusetts, Amherst), and ap$^{VNC}$–GAL4 was generated in our lab. *Snap* mutants were obtained from Dr. L.J. Pallanck (Univ. Washington, Seattle), and *Rop*, *Syx*, *vha* mutants were generated in the Bellen lab. *Dmca1D*$^{X10}$ mutants were obtained from Dr. L. Hall (Univ. California, Davis) and *Dmca1A*$^{HC129}$ mutants were obtained from Dr. R. Ordway (Penn State Univ.).

### Western Blot Analysis

To assess htt protein levels, pUAST-htt lines were crossed with the GMR-Gal4 driver at 27°C. Eight females per genotype were aged 1 day before isolating heads and homogenizing in sample buffer containing 8 M urea followed by boiling. Proteins were separated on 4%–20% gradient SDS/PAGE gels (BIO-RAD). After electrophoresis, gels were electroblotted overnight onto nitrocellulose membranes. The membranes were immunoblotted with anti-htt (MAB2166, Chemicon) at 1:2000, and immunoreactive bands were visualized using ECL western blotting detection reagents from Amersham. Densitometry analysis was done using a Molecular Dynamics Personal Densitometer SI and analyzed with Image Quant 5.2 software.

### Immunohistochemistry and Histology

Immunohistochemistry was performed as described (Fernandez-Funez et al., 2000; Verstreken et al., 2003) with the following modifications. Larvae and adult tissue was fixed in 4% formaldehyde for 1 hr and washed in 1XPBS with 0.1% Triton X-100. For GluRIIA labeling, larvae were fixed in 50% picric acid, 2.5% formaldehyde in 1XPBS for 20 min, and washed in 1XPBS with 0.1% Triton X-100. After blocking with 2% BSA, samples were incubated with primary antibodies overnight. Primary antibodies were used at the following concentrations: htt MAB5374 (1:200, Chemicon), HRP (1:500), GFP (1:200), Syt (1:200), Dlg (1:200), GluIIRA (1:100), Rop (1:100), SNAP (1:100), and syntaxin (1:200). After washing steps, secondary antibodies conjugated to Cy3 or Alexa 488 (Jackson Immunolabs, Molecular Probes) were used at 1:200.

Phalloidin staining to monitor rhabdomere degeneration was performed as described (Sang and Ready, 2002). Adult eye retinas were removed from the head capsule in 4% formaldehyde and fixed for 1 hr. Fixed, dissected eyes were washed in PBS, 0.1% Triton X-100 and incubated in phalloidin (1:200, Molecular Probes).

For visualizing the neuronal projections into IFMs, fixed adult thoraxes from 25-day-old adult flies were dissected along the midline, and neurons were labeled with anti-HRP antibody. The number of neuronal projections was counted in confocal stacks of a specified 100 μm × 100 μm area of IFMs 3 and 4 (located 100 μm away from the cuticle, shown in Figure 3D) using the whole-mount preparation of each hemithorax.

All immunostained samples were visualized using a Zeiss 510 confocal microscope, and ImageJ Software was used to obtain a 2D image by stacking the optically sectioned images. These stacked images were used for further analysis. Image panels were processed using Photoshop.

For light microscopy images, whole flies were frozen at −20°C. Photos were taken with a Leica MZ16 stereomicroscope using a MagnaFire SP Digital Camera, and images were collected with Image-Pro Plus 4.5 Analytical Imaging Software. For SEM images, whole flies were dehydrated in ethanol, critical-point dried, and analyzed with a JEOL JSM 6100 E.M.

### Adult Behavioral Assays

Climbing assays were performed on virgin female flies. Approximately 30 flies were placed in a plastic vial and gently tapped to the bottom of the vial. The number of flies above the 5 cm line after 18 s were counted and recorded. Ten trials were performed at each time point. The results shown represent the performance of one batch of flies tested over 30 days.

Flying tests were performed on 25-day-old female virgins. Flying ability was estimated by measuring flying distances after they were dropped from the top of a transparent plastic cylinder as described (Pesah et al., 2004).

### Larval Electrophysiological Assays

Third-instar physiology was performed as described (Verstreken et al., 2003). L3 NMJ recordings were performed in modified HL3 containing 110 mM NaCl, 5 mM KCl, 10 mM $NaHCO_3$, 5 mM HEPES, 30 mM sucrose, 5 mM trehalose, 5 mM $CaCl_2$, and 20 mM $MgCl_2$ (pH 7.2). mEJPs were recorded in modified HL-3 with 5 μM TTX and 0.5 mM $Ca^{2+}$. Current-clamp recordings were made from muscles 6 or 7 using high-resistance electrodes (100 MΩ) filled with 2 M KAc and 0.2 M KCl. EJPs were evoked at two times to three times threshold using a suction electrode. Data were digitized and stored on a PC with pClamp and analyzed with Clampfit (Axon) or Mini analysis (Synaptosoft). EJP amplitudes in low $Ca^{2+}$ were determined using only the successful events.

### Larval $Ca^{2+}$ Imaging

After dissecting larvae in Schneider's medium (GIBCO), a drop (~20 μl) of 5 mM Fura-2 Dextran (Invitrogen) was placed on the preparation, and a small amount of dye as well as a cut motor axon taken into a suction electrode. Excess dye was removed and the preparation washed and incubated in Schneider's medium for ~40 min. Following dye loading, Schneider's medium was replaced with modified HL3 containing 110 mM NaCl, 5 mM KCl, 10 mM $NaHCO_3$, 5 mM HEPES, 30 mM sucrose, 5 mM trehalose, and 20 mM $MgCl_2$ (pH 7.2), with 1 mM $Ca^{2+}$. Images were obtained after allowing the preparation to equilibrate with HL3 for ~15 min. Excitation at 340 nm and 380 nm was aided by a filter wheel (Sutter Lambda 10-2) and fluorescence images collected using a 40× water-immersion objective (Zeiss Achroplan) and Zeiss AxioCam MRm CCD camera. Images were processed with Amira 2.2.

### Supplemental Data

The Supplemental Data for this article can be found online at http://www.neuron.org/cgi/content/full/57/1/27/DC1/.

## ACKNOWLEDGMENTS

We thank R. Atkinson, the Baylor MRDDRC core (HD24062), and J. Barish for assistance with the laser confocal and SE microscopes; A. Singh for help with the plastic resin sections; A. Fayyazuddin for advice on the adult NMJ; and H.Y. Zoghbi for comments on the manuscript. Thanks to the Developmental Studies Hybridoma Bank for antibodies, the Bloomington Drosophila Stock Center, P. Jin, V. Budnik, Leo Pallanck, Linda Hall, and Richard Ordway for mutant strains, to D. Tagle for human htt cDNA. C.V.L. is supported by an NRSA fellowship from the NINDS (F30NS056520). G.-H.C. was supported by an HDSA fellowship and a postdoctoral fellowship from KOSEF. P.V. was supported by an R.L. Kirchstein NRS award, and H.J.B. is an HHMI investigator. This work was supported by NINDS grant NS42179 to J.B.

Received: November 17, 2006
Revised: June 21, 2007
Accepted: November 6, 2007
Published: January 9, 2008

## REFERENCES

Bezprozvanny, I., and Hayden, M.R. (2004). Deranged neuronal calcium signaling and Huntington disease. Biochem. Biophys. Res. Commun. *322*, 1310–1317.

Bilen, J., and Bonini, N.M. (2005). Drosophila as a model for human neurodegenerative disease. Annu. Rev. Genet. *39*, 153–171.

Brand, A.H., and Perrimon, N. (1993). Targeted gene expression as a means of altering cell fates and generating dominant phenotypes. Development *118*, 401–415.

Cattaneo, E., Zuccato, C., and Tartari, M. (2005). Normal huntingtin function: an alternative approach to Huntington's disease. Nat. Rev. Neurosci. *6*, 919–930.

Cepeda, C., Ariano, M.A., Calvert, C.R., Flores-Hernandez, J., Chandler, S.H., Leavitt, B.R., Hayden, M.R., and Levine, M.S. (2001). NMDA receptor function in mouse models of Huntington disease. J. Neurosci. Res. *66*, 525–539.

Cepeda, C., Hurst, R.S., Calvert, C.R., Hernandez-Echeagaray, E., Nguyen, O.K., Jocoy, E., Christian, L.J., Ariano, M.A., and Levine, M.S. (2003). Transient and progressive electrophysiological alterations in the corticostriatal pathway in a mouse model of Huntington's disease. J. Neurosci. *23*, 961–969.

DiFiglia, M., Sapp, E., Chase, K., Schwarz, C., Meloni, A., Young, C., Martin, E., Vonsattel, J.P., Carraway, R., Reeves, S.A., et al. (1995). Huntingtin is a cytoplasmic protein associated with vesicles in human and rat brain neurons. Neuron *14*, 1075–1081.

DiFiglia, M., Sapp, E., Chase, K.O., Davies, S.W., Bates, G.P., Vonsattel, J.P., and Aronin, N. (1997). Aggregation of huntingtin in neuronal intranuclear inclusions and dystrophic neurites in brain. Science *277*, 1990–1993.

Fergestad, T., Ganetzky, B., and Palladino, M.J. (2006). Neuropathology in Drosophila membrane excitability mutants. Genetics *172*, 1031–1042.

Fernandez-Funez, P., Nino-Rosales, M.L., de Gouyon, B., She, W.C., Luchak, J.M., Martinez, P., Turiegano, E., Benito, J., Capovilla, M., Skinner, P.J., et al. (2000). Identification of genes that modify ataxin-1-induced neurodegeneration. Nature *408*, 101–106.

Gatchel, J.R., and Zoghbi, H.Y. (2005). Diseases of unstable repeat expansion: mechanisms and common principles. Nat. Rev. Genet. *6*, 743–755.

Gauthier, L.R., Charrin, B.C., Borrell-Pagès, M., Dompierre, J.P., Rangone, H., Cordelières, F.P., De Mey, J., MacDonald, M.E., Lessmann, V., Humbert, S., et al. (2004). Huntingtin controls neurotrophic support and survival of neurons by enhancing BDNF vesicular transport along microtubules. Cell *118*, 127–138.

Goehler, H., Lalowski, M., Stelzl, U., Waelter, S., Stroedicke, M., Worm, U., Droege, A., Lindenberg, K.S., Knoblich, M., Haenig, C., et al. (2004). A protein interaction network links GIT1, an enhancer of huntingtin aggregation, to Huntington's disease. Mol. Cell *15*, 853–865.

Gunawardena, S., and Goldstein, L.S. (2005). Polyglutamine diseases and transport problems: deadly traffic jams on neuronal highways. Arch. Neurol. *62*, 46–51.

Gunawardena, S., Her, L.S., Brusch, R.G., Laymon, R.A., Niesman, I.R., Gordesky-Gold, B., Sintasath, L., Bonini, N.M., and Goldstein, L.S. (2003). Disruption of axonal transport by loss of huntingtin or expression of pathogenic polyQ proteins in Drosophila. Neuron *40*, 25–40.

Harjes, P., and Wanker, E.E. (2003). The hunt for huntingtin function: interaction partners tell many different stories. Trends Biochem. Sci. *28*, 425–433.

Hickey, M.A., and Chesselet, M.F. (2003). The use of transgenic and knock-in mice to study Huntington's disease. Cytogenet. Genome Res. *100*, 276–286.

Hiesinger, P.R., Fayyazuddin, A., Mehta, S.Q., Rosenmund, T., Schulze, K.L., Zhai, R.G., Verstreken, P., Cao, Y., Zhou, Y., Kunz, J., and Bellen, H.J. (2005). The v-ATPase V0 subunit a1 is required for a late step in synaptic vesicle exocytosis in Drosophila. Cell *121*, 607–620.

Hodgson, J.G., Agopyan, N., Gutekunst, C.A., Leavitt, B.R., LePiane, F., Singaraja, R., Smith, D.J., Bissada, N., McCutcheon, K., Nasir, J., et al. (1999). A YAC mouse model for Huntington's disease with full-length mutant

huntingtin, cytoplasmic toxicity, and selective striatal neurodegeneration. Neuron *23*, 181–192.

Jackson, G.R., Salecker, I., Dong, X., Yao, X., Arnheim, N., Faber, P.W., MacDonald, M.E., and Zipursky, S.L. (1998). Polyglutamine-expanded human huntingtin transgenes induce degeneration of Drosophila photoreceptor neurons. Neuron *21*, 633–642.

Kaltenbach, L.S., Romero, E., Becklin, R.R., Chettier, R., Bell, R., Phansalkar, A., Strand, A., Torcassi, C., Savage, J., Hurlburt, A., et al. (2007). Huntingtin interacting proteins are genetic modifiers of neurodegeneration. PLoS Genet. *3*, e82.

Katz, B., and Miledi, R. (1965). The effect of calcium on acetylcholine release from motor nerve terminals. Proc. R. Soc. Lond. B. Biol. Sci. *161*, 496–503.

Kawasaki, F., Felling, R., and Ordway, R.W. (2000). A temperature-sensitive paralytic mutant defines a primary synaptic calcium channel in Drosophila. J. Neurosci. *20*, 4885–4889.

Klapstein, G.J., Fisher, R.S., Zanjani, H., Cepeda, C., Jokel, E.S., Chesselet, M.F., and Levine, M.S. (2001). Electrophysiological and morphological changes in striatal spiny neurons in R6/2 Huntington's disease transgenic mice. J. Neurophysiol. *86*, 2667–2677.

Laforet, G.A., Sapp, E., Chase, K., McIntyre, C., Boyce, F.M., Campbell, M., Cadigan, B.A., Warzecki, L., Tagle, D.A., Reddy, P.H., et al. (2001). Changes in cortical and striatal neurons predict behavioral and electrophysiological abnormalities in a transgenic murine model of Huntington's disease. J. Neurosci. *21*, 9112–9123.

Lee, W.C., Yoshihara, M., and Littleton, J.T. (2004). Cytoplasmic aggregates trap polyglutamine-containing proteins and block axonal transport in a Drosophila model of Huntington's disease. Proc. Natl. Acad. Sci. USA *101*, 3224–3229.

Li, J.Y., Plomann, M., and Brundin, P. (2003). Huntington's disease: a synaptopathy? Trends Mol. Med. *9*, 414–420.

Li, S.H., and Li, X.J. (2004a). Huntingtin and its role in neuronal degeneration. Neuroscientist *10*, 467–475.

Li, S.H., and Li, X.J. (2004b). Huntingtin-protein interactions and the pathogenesis of Huntington's disease. Trends Genet. *20*, 146–154.

Lievens, J.C., Woodman, B., Mahal, A., and Bates, G.P. (2002). Abnormal phosphorylation of synapsin I predicts a neuronal transmission impairment in the R6/2 Huntington's disease transgenic mice. Mol. Cell. Neurosci. *20*, 638–648.

Marsh, J.L., and Thompson, L.M. (2004). Can flies help humans treat neurodegenerative diseases? Bioessays *26*, 485–496.

Menalled, L.B. (2005). Knock-in mouse models of Huntington's disease. NeuroRx *2*, 465–470.

Menalled, L.B., and Chesselet, M.F. (2002). Mouse models of Huntington's disease. Trends Pharmacol. Sci. *23*, 32–39.

Menalled, L.B., Sison, J.D., Wu, Y., Olivieri, M., Li, X.J., Li, H., Zeitlin, S., and Chesselet, M.F. (2002). Early motor dysfunction and striosomal distribution of huntingtin microaggregates in Huntington's disease knock-in mice. J. Neurosci. *22*, 8266–8276.

Murphy, K.P., Carter, R.J., Lione, L.A., Mangiarini, L., Mahal, A., Bates, G.P., Dunnett, S.B., and Morton, A.J. (2000). Abnormal synaptic plasticity and impaired spatial cognition in mice transgenic for exon 1 of the human Huntington's disease mutation. J. Neurosci. *20*, 5115–5123.

Nasir, J., Floresco, S.B., O'Kusky, J.R., Diewert, V.M., Richman, J.M., Zeisler, J., Borowski, A., Marth, J.D., Phillips, A.G., and Hayden, M.R. (1995). Targeted disruption of the Huntington's disease gene results in embryonic lethality and behavioral and morphological changes in heterozygotes. Cell *81*, 811–823.

Nicniocaill, B., Haraldsson, B., Hansson, O., O'Connor, W.T., and Brundin, P. (2001). Altered striatal amino acid neurotransmitter release monitored using microdialysis in R6/1 Huntington transgenic mice. Eur. J. Neurosci. *13*, 206–210.

Ordway, R.W., Pallanck, L., and Ganetzky, B. (1994). Neurally expressed Drosophila genes encoding homologs of the NSF and SNAP secretory proteins. Proc. Natl. Acad. Sci. USA *91*, 5715–5719.

Panov, A.V., Lund, S., and Greenamyre, J.T. (2005). Ca2+-induced permeability transition in human lymphoblastoid cell mitochondria from normal and Huntington's disease individuals. Mol. Cell. Biochem. *269*, 143–152.

Pennetta, G., Hiesinger, P.R., Fabian-Fine, R., Meinertzhagen, I.A., and Bellen, H.J. (2002). Drosophila VAP-33A directs bouton formation at neuromuscular junctions in a dosage-dependent manner. Neuron *35*, 291–306.

Pesah, Y., Pham, T., Burgess, H., Middlebrooks, B., Verstreken, P., Zhou, Y., Harding, M., Bellen, H., and Mardon, G. (2004). Drosophila parkin mutants have decreased mass and cell size and increased sensitivity to oxygen radical stress. Development *131*, 2183–2194.

Rubinsztein, D.C. (2002). Lessons from animal models of Huntington's disease. Trends Genet. *18*, 202–209.

Sang, T.K., and Ready, D.F. (2002). Eyes closed, a Drosophila p47 homolog, is essential for photoreceptor morphogenesis. Development *129*, 143–154.

Sang, T.K., and Jackson, G.R. (2005). Drosophila models of neurodegenerative disease. NeuroRx *2*, 438–446.

Schulze, K.L., Littleton, J.T., Salzberg, A., Halachmi, N., Stern, M., Lev, Z., and Bellen, H.J. (1994). rop, a Drosophila homolog of yeast Sec1 and vertebrate n-Sec1/Munc-18 proteins, is a negative regulator of neurotransmitter release in vivo. Neuron *13*, 1099–1108.

Schulze, K.L., Broadie, K., Perin, M.S., and Bellen, H.J. (1995). Genetic and electrophysiological studies of Drosophila syntaxin-1A demonstrate its role in nonneuronal secretion and neurotransmission. Cell *80*, 311–320.

Schuster, C.M., Ultsch, A., Schloss, P., Cox, J.A., Schmitt, B., and Betz, H. (1991). Molecular cloning of an invertebrate glutamate receptor subunit expressed in Drosophila muscle. Science *254*, 112–114.

Slow, E.J., van Raamsdonk, J., Rogers, D., Coleman, S.H., Graham, R.K., Deng, Y., Oh, R., Bissada, N., Hossain, S.M., Yang, Y.Z., et al. (2003). Selective striatal neuronal loss in a YAC128 mouse model of Huntington disease. Hum. Mol. Genet. *12*, 1555–1567.

Slow, E.J., Graham, R.K., Osmand, A.P., Devon, R.S., Lu, G., Deng, Y., Pearson, J., Vaid, K., Bissada, N., Wetzel, R., et al. (2005). Absence of behavioral abnormalities and neurodegeneration in vivo despite widespread neuronal huntingtin inclusions. Proc. Natl. Acad. Sci. USA *102*, 11402–11407.

Smith, R., Brundin, P., and Li, J.Y. (2005). Synaptic dysfunction in Huntington's disease: a new perspective. Cell. Mol. Life Sci. *62*, 1901–1912.

Steffan, J.S., Bodai, L., Pallos, J., Poelman, M., McCampbell, A., Apostol, B.L., Kazantsev, A., Schmidt, E., Zhu, Y.Z., Greenwald, M., et al. (2001). Histone deacetylase inhibitors arrest polyglutamine-dependent neurodegeneration in Drosophila. Nature *413*, 739–743.

Steffan, J.S., Agrawal, N., Pallos, J., Rockabrand, E., Trotman, L.C., Slepko, N., Illes, K., Lukacsovich, T., Zhu, Y.Z., Cattaneo, E., et al. (2004). SUMO modification of Huntingtin and Huntington's disease pathology. Science *304*, 100–104.

Sugars, K.L., and Rubinsztein, D.C. (2003). Transcriptional abnormalities in Huntington disease. Trends Genet. *19*, 233–238.

Swayne, L.A., Chen, L., Hameed, S., Barr, W., Charlesworth, E., Colicos, M.A., Zamponi, G.W., and Braun, J.E. (2005). Crosstalk between huntingtin and syntaxin 1A regulates N-type calcium channels. Mol. Cell. Neurosci. *30*, 339–351.

Szebenyi, G., Morfini, G.A., Babcock, A., Gould, M., Selkoe, K., Stenoien, D.L., Young, M., Faber, P.W., MacDonald, M.E., McPhaul, M.J., et al. (2003). Neuropathogenic forms of huntingtin and androgen receptor inhibit fast axonal transport. Neuron *40*, 41–52.

Tang, T.S., Tu, H., Chan, E.Y., Maximov, A., Wang, Z., Wellington, C.L., Hayden, M.R., and Bezprozvanny, I. (2003). Huntingtin and huntingtin-associated protein 1 influence neuronal calcium signaling mediated by inositol-(1,4,5) triphosphate receptor type 1. Neuron *39*, 227–239.

Tang, T.S., Slow, E., Lupu, V., Stavrovskaya, I.G., Sugimori, M., Llinas, R., Kristal, B.S., Hayden, M.R., and Bezprozvanny, I. (2005). Disturbed Ca2+ signaling and apoptosis of medium spiny neurons in Huntington's disease. Proc. Natl. Acad. Sci. USA *102*, 2602–2607.

The Huntington's Disease Collaborative Research Group (1993). A novel gene containing a trinucleotide repeat that is expanded and unstable on Huntington's disease chromosomes. Cell *72*, 971–983.

Usdin, M.T., Shelbourne, P.F., Myers, R.M., and Madison, D.V. (1999). Impaired synaptic plasticity in mice carrying the Huntington's disease mutation. Hum. Mol. Genet. *8*, 839–846.

Van Raamsdonk, J.M., Murphy, Z., Slow, E.J., Leavitt, B.R., and Hayden, M.R. (2005). Selective degeneration and nuclear localization of mutant huntingtin in the YAC128 mouse model of Huntington disease. Hum. Mol. Genet. *14*, 3823–3835.

Velier, J., Kim, M., Schwarz, C., Kim, T.W., Sapp, E., Chase, K., Aronin, N., and DiFiglia, M. (1998). Wild-type and mutant huntingtins function in vesicle trafficking in the secretory and endocytic pathways. Exp. Neurol. *152*, 34–40.

Verstreken, P., Koh, T.W., Schulze, K.L., Zhai, R.G., Hiesinger, P.R., Zhou, Y., Mehta, S.Q., Cao, Y., Roos, J., and Bellen, H.J. (2003). Synaptojanin is recruited by endophilin to promote synaptic vesicle uncoating. Neuron *40*, 733–748.

Waters, M.F., Minassian, N.A., Stevanin, G., Figueroa, K.P., Bannister, J.P., Nolte, D., Mock, A.F., Evidente, V.G., Fee, D.B., Müller, U., et al. (2006). Mutations in voltage-gated potassium channel KCNC3 cause degenerative and developmental central nervous system phenotypes. Nat. Genet. *38*, 447–451.

Wu, M.N., Littleton, J.T., Bhat, M.A., Prokop, A., and Bellen, H.J. (1998). ROP, the Drosophila Sec1 homolog, interacts with syntaxin and regulates neurotransmitter release in a dosage-dependent manner. EMBO J. *17*, 127–139.

Yu, Z.X., Li, S.H., Evans, J., Pillarisetti, A., Li, H., and Li, X.J. (2003). Mutant huntingtin causes context-dependent neurodegeneration in mice with Huntington's disease. J. Neurosci. *23*, 2193–2202.

Zeron, M.M., Hansson, O., Chen, N., Wellington, C.L., Leavitt, B.R., Brundin, P., Hayden, M.R., and Raymond, L.A. (2002). Increased sensitivity to N-methyl-D-aspartate receptor-mediated excitotoxicity in a mouse model of Huntington's disease. Neuron *33*, 849–860.

Zheng, W., Feng, G., Ren, D., Eberl, D.F., Hannan, F., Dubald, M., and Hall, L.M. (1995). Cloning and characterization of a calcium channel alpha 1 subunit from Drosophila melanogaster with similarity to the rat brain type D isoform. J. Neurosci. *15*, 1132–1143.